




TIGIT deficiency promotes autoreactive CD4⁺ T-cell responses through a metabolic–epigenetic mechanism in autoimmune myositis

Received: 12 August 2024

Accepted: 30 April 2025

Published online: 15 May 2025



Yimei Lai^{1,7}, Shuang Wang^{1,7}, Tingting Ren^{1,7} , Jia Shi¹, Yichao Qian^{1,2}, Shuyi Wang^{1,2}, Mianjing Zhou¹, Ryu Watanabe³, Mengyuan Li¹, Xinyuan Ruan¹, Xin Wang⁴, Lili Zhuang¹, Zunfu Ke^{2,5,6}, Niansheng Yang¹, Yuefang Huang⁴ & Hui Zhang^{1,2}  

Polymyositis (PM) is a systemic autoimmune disease characterized by muscular inflammatory infiltrates and degeneration. T-cell immunoreceptor with Ig and ITIM domains (TIGIT) contributes to immune tolerance by inhibiting T cell-mediated autoimmunity. Here, we show that a reduced expression of TIGIT in CD4⁺ T cells from patients with PM promotes these cells' differentiation into Th1 and Th17 cells, which could be rescued by TIGIT over-expression. Knockout of TIGIT enhances muscle inflammation in a mouse model of experimental autoimmune myositis. Mechanistically, we find that TIGIT deficiency enhances CD28-mediated PI3K/AKT/mTOR co-stimulatory pathway, which promotes glucose oxidation, citrate production, and increased cytosolic acetyl-CoA levels, ultimately inducing epigenetic reprogramming via histone acetylation. Importantly, pharmacological inhibition of histone acetylation suppresses the differentiation of Th1 and Th17 cells, alleviating muscle inflammation. Thus, our findings reveal a mechanism by which TIGIT directly affects the differentiation of Th1 and Th17 T cells through metabolic–epigenetic reprogramming, with important implications for treating systemic autoimmune diseases.

Polymyositis (PM), an autoimmune myositis, is characterized by chronic muscle inflammation and degeneration. The predominance of T cells among inflammatory infiltrates in muscle biopsies underscores the critical role of autoreactive T-cell responses in the pathogenesis of PM^{1,2}. The underlying mechanisms that drive autoreactive T-cell responses in PM remain largely unclear.

Two distinct proinflammatory CD4⁺ T helper (Th) cell subsets, Th1 and Th17 cells, play pivotal roles in tissue inflammation in various autoimmune diseases. IFN γ -producing Th1 cells activate proinflammatory M1-like microglia, thereby promoting the pathogenesis of multiple sclerosis³. Therapies targeting Th17 cell effector cytokines have shown clinical efficacy in treating diseases such as psoriasis,

¹Department of Rheumatology and Clinical immunology, the First Affiliated Hospital of Sun Yat-sen University, Guangzhou, China. ²Institute of Precision Medicine, the First Affiliated Hospital of Sun Yat-sen University, Guangzhou, China. ³Department of Clinical Immunology, Osaka Metropolitan University Graduate School of Medicine, Osaka, Japan. ⁴Department of Pediatrics, the First Affiliated Hospital of Sun Yat-sen University, Guangzhou, China. ⁵Department of Pathology, the First Affiliated Hospital of Sun Yat-Sen University, Guangzhou, China. ⁶Molecular Diagnosis and Gene Test Centre, the First Affiliated Hospital of Sun Yat-Sen University, Guangzhou, China. ⁷These authors contributed equally: Yimei Lai, Shuang Wang, Tingting Ren. ✉ e-mail: zhangh656@mail.sysu.edu.cn

psoriatic arthritis, and axial spondyloarthritis^{4–6}. IL-17-positive and IFN γ -positive cells have been detected in muscle infiltrates in patients with PM^{7–9}. Our previous study revealed significant expansion of Th1 and Th17 cells in the peripheral blood of patients with PM, and the inhibition of Th1 and Th17 cell differentiation reduced muscle inflammation in mice with experimental autoimmune myositis (EAM)¹⁰.

Cellular metabolism is intrinsically linked to T-cell proliferation and effector functions in health and disease^{11,12}. Naive T cells exhibit low-level catabolism, fueled by amino acids and fatty acids for ATP generation. Upon activation, T cells undergo metabolic reprogramming, and glucose metabolism is rapidly increased to meet energy requirements. In addition, mitochondrial metabolism and oxidative phosphorylation are increased simultaneously^{13,14}. Glycolysis provides important metabolic intermediates, which are not only the building blocks of biosynthesis or energy production but also interact with important signals in T cells¹⁵. It has been shown that cellular metabolism influences Th cell differentiation via epigenetic modifications¹². Recently, it has been reported that polyamine metabolism regulates acetyl-CoA production and epigenetic remodeling in CD4⁺ T cells and thus induces Th-cell differentiation¹⁵. Besides, glucose glycolysis could modify histone acetylation to control Th1 cell differentiation¹⁶. Ablation of *Glut3* in CD4⁺ T cells leads to reduced acetyl-CoA production and histone acetylation, resulting in impaired Th17 differentiation¹⁷. Autoreactive T cells exhibit enhanced glucose metabolism. Inhibition of glycolysis reduced autoreactive Th1/Th17 responses and ameliorated autoimmune diseases in mouse models^{18–20}. How the fates of these autoreactive T cells are determined metabolically is not clear, and their underlying mechanisms are poorly understood.

T-cell immunoreceptor with Ig and ITIM domains (TIGIT) is a newly identified co-inhibitory immune checkpoint that contributes to immune evasion in cancer²¹. TIGIT belongs to the poliovirus receptor family and is expressed primarily on activated T cells, NK cells, memory T cells, and Tregs²². Its ligands include CD155 (PVR), CD112 (PVRL2), and CD113, which are expressed mainly on antigen-presenting cells or tumor cells. TIGIT binds to CD155 with the highest affinity and competes with CD226 and CD96, which bind the same ligands with lower affinity²³. TIGIT contains an immunoreceptor tyrosine-based inhibitory motif (ITIM) and an immunoreceptor tail tyrosine (ITT)-like motif^{24,25}. Thus, TIGIT can exert inhibitory effects on T-cell responses in a cell-intrinsic manner^{26,27}. In addition, TIGIT exhibits inhibitory effects on T cells by inducing tolerogenic dendritic cells (DC) or by indirectly enhancing Treg function^{22,28}. TIGIT impairs the dimerization of CD226 and prevents CD226 from binding to CD155, thereby hindering CD226-mediated T-cell activation²⁹. TIGIT knockout mice develop more severe experimental autoimmune encephalitis when challenged with myelin oligodendrocyte glycoprotein²⁶. Soluble TIGIT is also able to ameliorate inflammatory responses and disease activities in lupus mice³⁰. Nonetheless, the precise role and pathophysiological significance of TIGIT in autoimmune diseases remain elusive. The effects of cell-intrinsic TIGIT on Th cell differentiation in autoimmune diseases need to be further elucidated.

Here, we show that reduced TIGIT expression in CD4⁺ T cells from patients with PM unleashes the differentiation of Th1 and Th17 cells through metabolic–epigenetic reprogramming. Mechanistically, we find that cell-intrinsic TIGIT inhibits CD28-mediated PI3K/AKT/mTOR signaling in CD4⁺ T cells. Thus, these findings implicate TIGIT in the maintenance of immune homeostasis and suggest that TIGIT could serve as a critical metabolic–epigenetic checkpoint to control autoreactive CD4⁺ T-cell responses in autoimmune diseases.

Results

TIGIT deficiency in CD4⁺ T cells from patients with PM

TIGIT is an immune receptor that is expressed on activated T cells, Tregs, and NK cells. TIGIT shares the common ligand CD155 with CD226 and CD96 and exerts inhibitory effects on T-cell responses (Fig. 1a)²¹. The role of TIGIT in patients with PM remains elusive. To

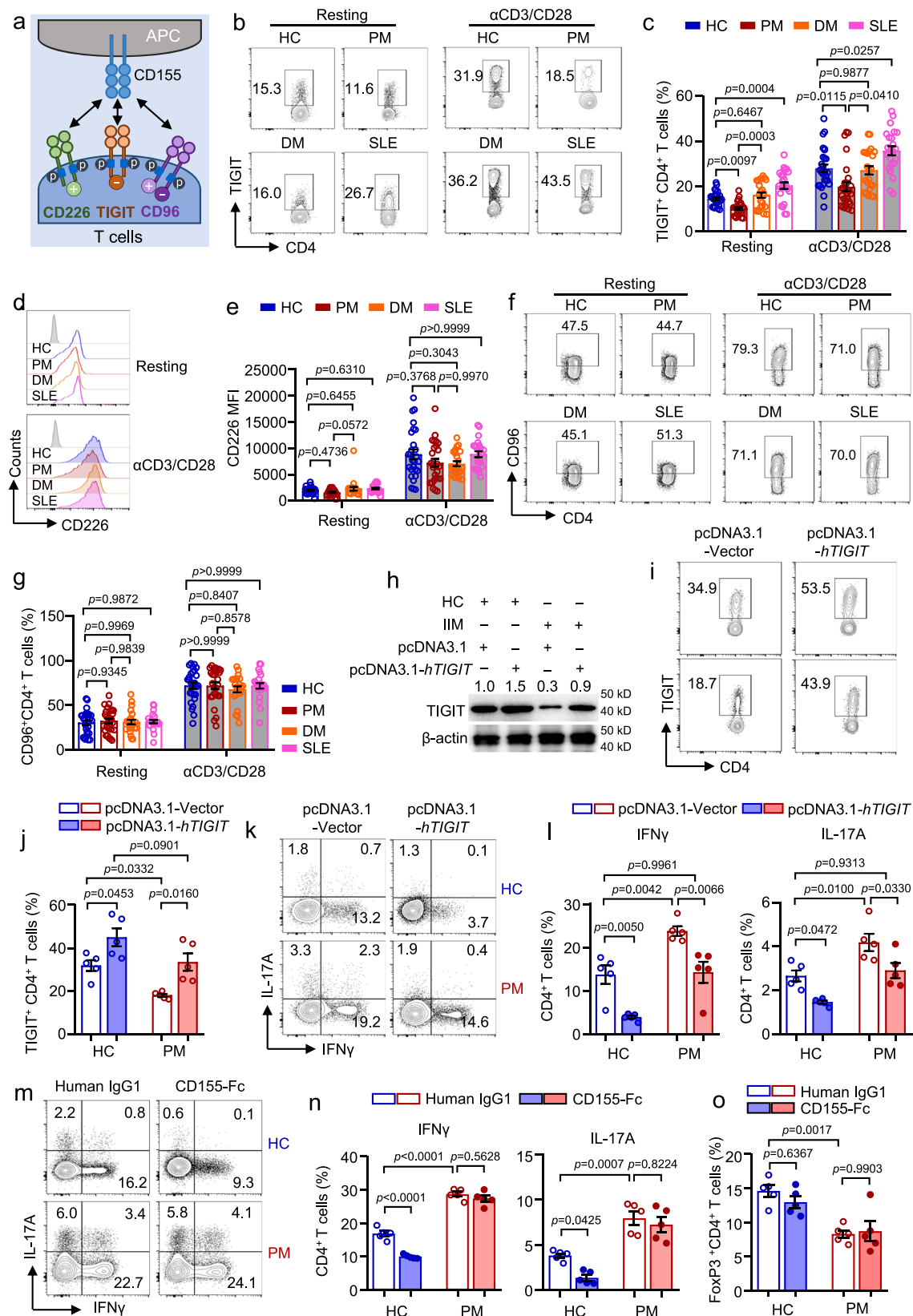
explore the potential role of TIGIT in patients with PM, we quantified the expression of TIGIT, CD226, and CD96 in T cells isolated from patients with PM and healthy controls (HC) by flow cytometry. Patients with dermatomyositis (DM) or systemic lupus erythematosus (SLE) were recruited as disease controls. We found that TIGIT expression was significantly lower in CD4⁺ T cells from patients with PM than in those from HC. Total CD4⁺ T cells were then activated with anti-CD3/CD28 beads. The expression of TIGIT in CD4⁺ T cells from both PM and HC was dramatically upregulated when T cells were activated by anti-CD3/CD28 beads. Interestingly, TIGIT expression in CD4⁺ T cells from PM patients was increased to a notably lesser extent than that in CD4⁺ T cells from HC (Fig. 1b, c). In contrast, CD4⁺ T cells from patients with SLE showed enhanced TIGIT expression. While TIGIT expression in CD4⁺ T cells from DM showed a similar level to that of HC (Fig. 1b, c). No difference was observed in the expression of CD226 and CD96 in CD4⁺ T cells from patients with PM, DM, or SLE in the resting state. Although T-cell activation by anti-CD3/CD28 beads led to profound upregulation of CD226 and CD96, the expression of CD226 and CD96 was similar in CD4⁺ T cells from patients with PM, DM, SLE, and HC (Fig. 1d–g). CD8⁺ T cells play a role in the pathogenesis of PM. The expression of TIGIT, CD226, and CD96 in resting or activated CD8⁺ T cells was comparable between PM patients and HC (Supplementary Fig. 1a–g). The expression of CD226 and CD96 in CD8⁺ T cells from patients with DM and SLE was also unchanged (Supplementary Fig. 1a–g). We observed slightly reduced TIGIT expression in NK cells from PM (Supplementary Fig. 1h, i). CD155 serves as the major ligand of TIGIT and is expressed mainly by monocytes and DCs in the peripheral blood. However, CD155 expression was similar between monocytes and DCs from PM compared to that of HC (Supplementary Fig. 2a–e). The expression of CD155 in T cells was also not different between PM patients and HC (Supplementary Fig. 2f, g).

TIGIT deficiency drives proinflammatory CD4⁺ T-cell responses in PM

TIGIT plays an important role in controlling T-cell responses. The defect in TIGIT expression could lead to enhanced inflammatory CD4⁺ T-cell responses in PM. In line with this hypothesis, the activation markers CD44, CD25, and HLA-DR were induced to much higher levels in CD4⁺ T cells from PM patients than in those from HC (Supplementary Fig. 3a, b). In addition, CD4⁺ T cells from PM patients proliferated faster than did CD4⁺ T cells from HC when stimulated with anti-CD3/CD28 beads (Supplementary Fig. 3c, d). Notably, the percentages of IFN γ ⁺ and IL-17A⁺ CD4⁺ T cells were 2.1 and 1.7 times higher in PM patients than in HC, respectively (Supplementary Fig. 3e, f). Th2 cell-associated cytokines were even lower in CD4⁺ T cells from PM (Supplementary Fig. 3g–k).

Intriguingly, we observed that TIGIT was predominantly downregulated in IFN γ - and IL-17A-producing CD4⁺ T cells in PM (Supplementary Fig. 4a–c). Furthermore, the extent of TIGIT downregulation was strongly correlated with the frequencies of IFN γ - and IL-17A-producing CD4⁺ T cells and disease activities as determined by physician VAS, patient/parent VAS, myositis disease activity assessment visual analog scales (MYOACT), extramuscular element³¹, MMT-8³¹, and creatine kinase (CK) levels (Supplementary Fig. 4d–f, Supplementary Fig. 5).

To address whether TIGIT deficiency is causative of hyperinflammatory CD4⁺ T-cell responses in PM, TIGIT was overexpressed in CD4⁺ T cells from PM and HC (Fig. 1h–j). The data revealed that overexpression of TIGIT decreased IFN γ and IL-17A production in HC CD4⁺ T cells. Intriguingly, the production of IFN γ and IL-17A in CD4⁺ T cells of PM patients was similar to that in CD4⁺ T cells of HC when TIGIT expression was rescued in patient CD4⁺ T cells (Fig. 1k, l). We further cultured CD4⁺ T cells from PM or HC with recombinant human CD155-Fc. The data revealed that TIGIT engagement by CD155-Fc decreased IFN γ and IL-17A production in CD4⁺ T cells from HC by 41.1% and 64.8%,



respectively. However, the expression of IFN γ and IL-17A in CD4⁺ T cells from PM was not affected by CD155-Fc (Fig. 1m, n). Consistently, Treg cells were lower in patients with PM than in HC. And the expression of FoxP3 was not changed by CD155-Fc in either HC or PM CD4⁺ T cells (Fig. 1o). Together, these data suggest that TIGIT deficiency contributes to hyperinflammatory CD4⁺ T-cell responses in PM.

TIGIT deficiency promotes Th1 and Th17 cell differentiation in PM

Naive human CD4⁺ T cells showed negative expression of TIGIT, which was upregulated dramatically from day 3 after stimulation by anti-CD3/CD28 (Fig. 2a, b). Considering the critical role of T-cell proliferation in determining CD4⁺ cell fate³², the upregulation of TIGIT alongside T-cell

Fig. 1 | TIGIT deficiency promotes proinflammatory CD4⁺ T cells in patients with PM. PBMCs were collected from polymyositis (PM), dermatomyositis (DM), systemic lupus erythematosus (SLE), or healthy controls (HC). TIGIT, CD226, and CD96 expression in cells in PBMCs was measured by flow cytometry. **a** Schematic employed to visualize TIGIT, CD226, and CD96 on T cells binding to CD155 on antigen-presenting cells (APC). **b–g** CD4⁺ T cells from HC or PM, DM or SLE patients were stimulated with anti-CD3/CD28 beads (α CD3/CD28) for 3 d. The expression of TIGIT, CD226, and CD96 in pre- and post-activation of CD4⁺ T cells was measured by flow cytometry of biological replicates (HC = 27, PM = 27, DM = 23, SLE = 23). **h** Naive CD4⁺ T cells isolated from PBMCs of HC or patients with PM, were stimulated with α CD3/CD28. TIGIT expression was measured by flow cytometry. Data from four biologically independent replicates. **h–i** Total CD4⁺ T cells from patients with PM or HC were transfected with pcDNA3.1-hTIGIT or pcDNA3.1-Vector by

electroporation. Cells were then stimulated by α CD3/CD28 for 3 d.

h Overexpression of TIGIT was confirmed by Western blot. The experiment was repeated three times independently with similar results. **i, j** Overexpression of TIGIT in CD4⁺ T cells from HC or PM was confirmed by flow cytometry. Data from five biologically independent replicates. **k, l** IFN γ and IL-17A production by CD4⁺ T cells from PM patients or HC was measured by flow cytometry. Data from five biologically independent replicates. **m–o** CD4⁺ T cells from PM patients or HC were stimulated with α CD3/CD28 in the presence of CD155-Fc (10 μ g/ml) or control IgG1 for 3 d. IFN γ , IL-17A, and FoxP3 expression in CD4⁺ T cells from PM patients or HC was measured by flow cytometry. Data from five biologically independent replicates. All data are mean \pm SEM. Statistics were done by one-way ANOVA with adjustments for multiple comparisons in **c, e, g**, and two-way ANOVA with adjustments for multiple comparisons in **j, l, n**, and **o**.

proliferation suggests that TIGIT might be involved in CD4⁺ cell differentiation. We then isolated naive CD4⁺ T cells from PM or HC to explore whether TIGIT has effects on human CD4⁺ T-cell differentiation. Surprisingly, the upregulation of TIGIT in naive CD4⁺ T cells from PM was notably lower than that in those from HC stimulated with anti-CD3/CD28 (Fig. 2a, b). TIGIT was then overexpressed in naive CD4⁺ T cells from PM and HC (Fig. 2c–i). Our data revealed that overexpression of TIGIT suppressed the differentiation of human Th1 and Th17 cells from naive CD4⁺ T cells (Fig. 2f–i). Intriguingly, these patient naive CD4⁺ T cells were prone to differentiate into Th1 and Th17 cells. Importantly, the differentiation of IFN γ ⁺ Th1 and IL-17A⁺ Th17 cells from PM naive CD4⁺ T cells was reduced to a level similar to that of those from HC when TIGIT expression was rescued in patient CD4⁺ T cells (Fig. 2f–i).

We further used CD155-Fc to investigate the cell-intrinsic function of TIGIT in human CD4⁺ T-cell differentiation. We found that TIGIT engagement by CD155-Fc led to decreased T-bet expression in CD4⁺ T cells from HC under Th1-polarizing conditions. The percentage of IFN γ ⁺ Th1 cells was much lower in the CD155-Fc-treated cells (Fig. 2j, k). The percentage of IL-17A⁺ Th17 cells was significantly lower in HC CD4⁺ cells treated with CD155-Fc under Th17-polarizing conditions (Fig. 2l, m). However, neither the differentiation of IFN γ ⁺ Th1 nor that of IL-17A⁺ Th17 cells from PM naive CD4⁺ T cells was affected by CD155-Fc (Fig. 2j–m), which might be due to a cell-intrinsic defect in TIGIT signaling in patient CD4⁺ T cells.

Knockdown of TIGIT in HC CD4⁺ T cells recapitulates the proinflammatory phenotype of patient CD4⁺ T cells

We next investigated whether knockdown of TIGIT in HC CD4⁺ T cells could recapitulate the proinflammatory phenotype of patient CD4⁺ T cells (Fig. 3a–c). Our data revealed that cell proliferation and cytokine production of IFN γ and IL-17A were both notably enhanced in CD4⁺ T cells when TIGIT was knocked down (Fig. 3d–i). Moreover, these TIGIT-deficient CD4⁺ T cells showed a tendency to differentiate into proinflammatory IFN γ ⁺ Th1 and IL-17A⁺ Th17 cells, resembling TIGIT^{low} T cells from PM patients. While Th2 cell differentiation was reduced in TIGIT knocked down CD4⁺ T cells, leaving FoxP3⁺ Treg cells unaffected (Fig. 3j–x). These data suggest the important role of TIGIT deficiency in driving proinflammatory T-cell responses in PM. TIGIT controls the differentiation of mouse Th1 and Th17 cells.

We next used *Tigit*^{−/−} mice to further investigate the role of TIGIT in CD4⁺ T-cell differentiation in vitro and in vivo (Supplementary Fig. 6a). In Naive CD4⁺ T cells from *Tigit*^{+/+} mice, TIGIT expression was slightly upregulated on day 1 and 2 by anti-CD3/CD28 stimulation, with robust induction on day 3 (Supplementary Fig. 6b, c). To further dissect whether cell-intrinsic TIGIT exerts direct effects on mouse CD4⁺ T-cell differentiation, we isolated naive CD4⁺ T cells from *Tigit*^{−/−} or *Tigit*^{+/+} mice and stimulated the cells under different polarizing conditions. Our data revealed that the expression of T-bet, the master transcription factor for Th1 cells, was upregulated in *Tigit*^{−/−} CD4⁺ T cells under Th1-polarizing conditions. Accordingly, IFN γ production

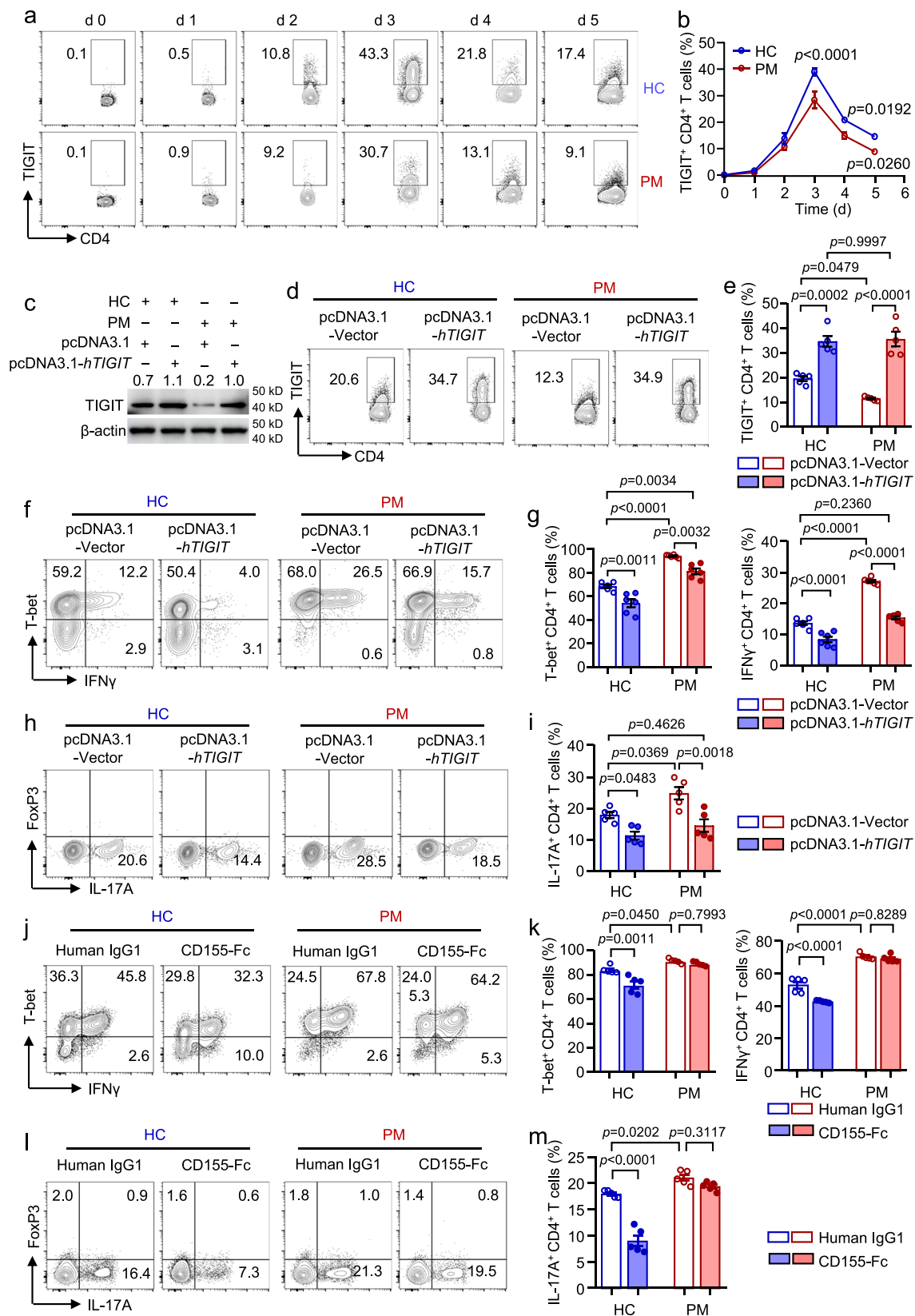
was profoundly increased in *Tigit*^{−/−} CD4⁺ T cells (Fig. 4a–d). In contrast, the expression of the transcription factor GATA3 in Th2 cells was reduced in *Tigit*^{−/−} CD4⁺ T cells under Th2-polarizing conditions. The expression of IL-4 was also lower in *Tigit*^{−/−} CD4⁺ T cells (Fig. 4e–h). Moreover, the expression of ROR γ t, the key transcription factor for Th17 cells, was increased in *Tigit*^{−/−} CD4⁺ T cells under the Th17-polarizing condition. Importantly, the number of IL-17A⁺ *Tigit*^{−/−} CD4⁺ T cells was 2.2 times greater than that of *Tigit*^{+/+} CD4⁺ T cells (Fig. 4i–l). Consistent with human data, no difference in FoxP3 expression was detected between *Tigit*^{−/−} and *Tigit*^{+/+} CD4⁺ T cells under Treg-polarizing conditions (Fig. 4m, n). We then performed RNA-seq to identify the differentially expressed genes (DEG) in *Tigit*^{−/−} CD4⁺ T cells. The RNA-seq data revealed that inflammatory responses and cytokine production were upregulated and enriched in *Tigit*^{−/−} CD4⁺ T cells (Supplementary Fig. 6d–k).

Next, *Rag1*^{−/−} mice were reconstituted with naive *Tigit*^{−/−} or *Tigit*^{+/+} CD4⁺ T cells and challenged with autologous myosin (Fig. 4o). Flow cytometry analysis revealed that T-bet⁺ and ROR γ t⁺ CD4⁺ T cells were notably expanded in mice that received naive *Tigit*^{−/−} CD4⁺ T cells (Fig. 4p, q). Importantly, the percentages of IFN γ ⁺ Th1 cells and IL-17A⁺ Th17 cells in mice that received naive *Tigit*^{−/−} CD4⁺ T cells were 2.1 and 2.0 times greater than those in mice that received *Tigit*^{+/+} CD4⁺ T cells, respectively (Fig. 4r, s). Mice received *Tigit*^{−/−} CD4⁺ T cells showed weaker muscle strength and enhanced spleen weight index. Importantly, mice receiving *Tigit*^{−/−} CD4⁺ T cells developed much severe disease, and muscle infiltrate was significantly increased in these mice (Fig. 4, Supplementary Fig. 6l–n). As a proof of concept, cell-intrinsic TIGIT controls the differentiation of CD4⁺ T cells. The data suggest that TIGIT deficiency directly promotes the differentiation of Th1 and Th17 cells and thus plays a role in the development of autoimmune myositis (Fig. 4t).

Knockout of TIGIT drives Th1 and Th17 expansion and promotes the development of EAM

TIGIT knockout mice were used to further explore the role of TIGIT in the development of autoimmune myositis. Knockout of TIGIT did not affect CD226 or CD96 expression in CD4⁺ T cells in the spleen (Supplementary Fig. 7). *Tigit*^{+/+}, *Tigit*^{+/−}, or *Tigit*^{−/−} mice were immunized with autologous myosin to induce EAM as previously described¹⁰ (Fig. 5a). Notably, the muscle strength of *Tigit*^{−/−} mice was much weaker than that of *Tigit*^{+/+} mice. Of note, muscle strength was similar between *Tigit*^{+/+} and *Tigit*^{+/−} mice (Fig. 5b). Both the spleen size and the spleen weight index were increased in *Tigit*^{−/−} mice. While the spleens of *Tigit*^{−/−} mice were not different to that of *Tigit*^{+/+} mice (Fig. 5c). Notably, the frequencies of IFN γ ⁺ and IL-17A-producing CD4⁺ T cells in the spleens were increased in *Tigit*^{−/−} mice (Fig. 5d, e). The expression of CD44, an activation marker of T cells, was also increased in CD4⁺ T cells from *Tigit*^{−/−} mice (Fig. 5f, g).

Next, bulk RNA-seq was performed on inflamed quadriceps muscles to reveal the inflammatory states in *Tigit*^{−/−} and *Tigit*^{+/+} mice. DEGs identified via RNA-seq were shown in a volcano plot in which the



expression of a cytokine regulatory gene (*Btn19*) and T-cell activation regulatory genes (*Ckmt2*, *Mapk10*) were upregulated in the quadriceps muscle of *Tigit*^{-/-} mice (Supplementary Fig. 8a). Pathway enrichment analysis suggested that TIGIT deficiency induced changes in overall inflammation (Supplementary Fig. 8b), and the differentiation of T cells, including Th1, Th2, and Th17 cells, was altered in the muscle

infiltrates of TIGIT knockout mice (Supplementary Fig. 8c). We applied qPCR to confirm the T-cell signatures in inflamed muscles and found that the mRNA transcript levels of *Ifng*, *Il17a*, *Il17f*, and *Il2* were notably increased in the inflamed quadriceps muscle of *Tigit*^{-/-} mice (Fig. 5h). HE staining revealed that inflammatory infiltrates were profoundly increased in the quadriceps of *Tigit*^{-/-} mice (Fig. 5i). These data

Fig. 2 | TIGIT deficiency promotes Th1 and Th17 cell differentiation in patients with PM. **a, b** Naive CD4⁺ T cells isolated from PBMCs from HC or PM patients were stimulated with α CD3/CD28 for 5 d. TIGIT expression in CD4⁺ T cells was measured by flow cytometry. Representative contour plots were shown. Data from four biologically independent replicates. **c–i** Naive CD4⁺ T cells from patients with PM or HC were transfected with pcDNA3.1-*hTIGIT* or pcDNA3.1-Vector by electroporation. Cells were then stimulated by α CD3/CD28 for 5 d. **c** Overexpression of TIGIT in CD4⁺ T cells from HC or PM was confirmed by western blot. The experiment was repeated three times independently with similar results. **d, e** Overexpression of TIGIT in CD4⁺ T cells from HC or PM was confirmed by flow cytometry. Data from five biologically independent replicates. **f, g** Naive CD4⁺ T cells were cultured and polarized under Th1 cell conditions for 5 d. IFN γ and T-bet expression in CD4⁺

T cells were measured by flow cytometry. Data from six biologically independent replicates. **h, i** Naive CD4⁺ T cells were cultured and polarized under Th17 cell conditions for 5 d. The expressions of FoxP3 and IL-17A were measured by flow cytometry, and data from five biologically independent replicates. **j, k** Naive CD4⁺ T cells were polarized in Th1 condition in the presence of recombinant human CD155-Fc (10 μ g/ml) or IgG1 control for 5 d. IFN γ and T-bet expression in CD4⁺ T cells were measured by flow cytometry. Data from five biologically independent replicates. **l, m** Naive CD4⁺ T cells polarized in Th17 condition in the presence of recombinant human CD155-Fc (10 μ g/ml) or IgG1 control for 5 d. IL-17A and FoxP3 expression in CD4⁺ T cells were measured by flow cytometry. Data from five biologically independent replicates. All data are mean \pm SEM. Statistics were done by two-way ANOVA followed by adjustments for multiple comparisons.

revealed that similar disease phenotypes of PM could be repeated in *Tigit*^{−/−} mice, suggesting the important role of TIGIT in the development of PM.

An anti-TIGIT agonistic antibody was used to treat EAM mice to validate the role of TIGIT in the development of autoimmune myositis (Fig. 5j). Consistently, TIGIT stimulation led to reduced disease severity, and muscle strength was greater in anti-TIGIT-treated mice than in control mice (Fig. 5k). Both the size of the spleen and the spleen weight index were decreased in the anti-TIGIT-treated mice (Fig. 5l). Moreover, the frequencies of IFN γ - and IL-17A-producing CD4⁺ T cells in the spleen were notably decreased after treatment (Fig. 5m–o). Accordingly, muscle infiltration was profoundly reduced by TIGIT stimulation (Fig. 5p, q). Together, TIGIT deficiency unleashes Th1 and Th17 cell responses and promotes the development of autoimmune myositis.

TIGIT controls Th1 and Th17 cell differentiation in a glycolysis-dependent manner

Our previous study has shown that glucose metabolism is upregulated in CD4⁺ T cells from patients with myositis¹⁰. To determine whether TIGIT deficiency contributes to enhanced glucose metabolism in PM CD4⁺ T cells, we first isolated *Tigit*^{−/−} or *Tigit*^{+/+} CD4⁺ T cells and incubated them with the glucose analog 2-NBDG and the lipid probes Bodipy 500 and Bodipy 493 for lipid uptake and lipid content, respectively. Flow cytometry analysis revealed that glucose uptake was notably increased in *Tigit*^{−/−} CD4⁺ T cells. No difference in lipid uptake or lipid content was detected between *Tigit*^{−/−} and *Tigit*^{+/+} CD4⁺ T cells (Supplementary Fig. 9). We further performed stable isotope tracing of polar metabolites to further dissect the role of TIGIT in glucose metabolism in CD4⁺ T cells. *Tigit*^{−/−} and *Tigit*^{+/+} CD4⁺ T cells were incubated with ¹³C-glucose and analyzed by gas chromatography (GC) coupled with mass spectrometry (MS) (Supplementary Fig. 10). ¹³C-glucose-derived metabolites in CD4⁺ T cells can be identified by the isotopic increase in their specific molecular mass (Fig. 6a). Notably, mitochondrial isotopologues (m + 2) were increased in *Tigit*^{−/−} CD4⁺ T cells, with significant upregulation of citrate, α -ketoglutarate, and malate (Fig. 6b). Accordingly, the mitochondrial oxygen consumption rate (OCR) was significantly increased in *Tigit*^{−/−} CD4⁺ T cells. Basal respiration, respiration coupled to ATP generation, maximal respiration, and spared respiratory capacity were all enhanced in *Tigit*^{−/−} CD4⁺ T cells (Fig. 6c). We also noticed that extracellular acidification rate (ECAR) was increased in *Tigit*^{−/−} CD4⁺ T cells (Fig. 6d). Glycolysis stress test further confirmed the overall enhanced glucose glycolysis in *Tigit*^{−/−} CD4⁺ T cells (Fig. 6e–h). However, the mitochondrial mass and mitochondrial potential did not differ between *Tigit*^{−/−} and *Tigit*^{+/+} CD4⁺ T cells (Supplementary Fig. 11).

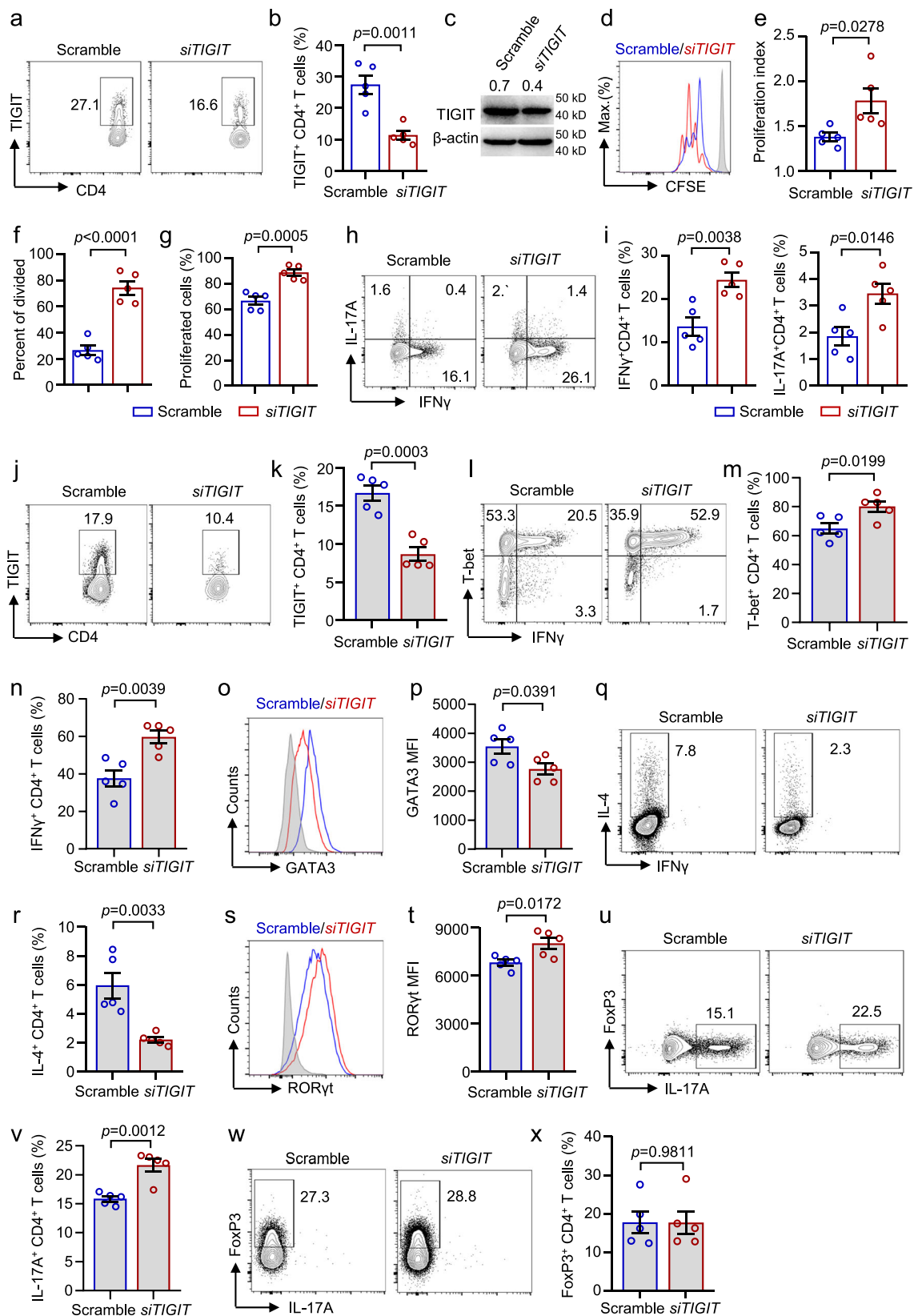
¹³C-glucose-derived metabolite tracing by liquid chromatography (LC) coupled with MS revealed that CD4⁺ T cells from patients with PM presented increased levels of glycolytic intermediates such as fructose 6-phosphate, fructose biphosphate, and phosphoenolpyruvate (Supplementary Fig. 10, Supplementary Fig. 12a, b). Notably, the levels of mitochondrial isotopologues (m + 2), including citrate, α -ketoglutarate, succinate, and malate, were increased in CD4⁺ T cells from

patients with PM (Supplementary Fig. 10, Supplementary Fig. 12c), suggesting that TIGIT deficiency might directly contribute to enhanced glucose metabolism in CD4⁺ T cells in PM. To further stress the effect of TIGIT on human cells, we cultured human CD4⁺ T cells isolated from HC peripheral blood mononuclear cells (PBMC) with anti-CD3/CD28 beads in the presence of CD155-FC for 3 d. The cells were subjected to a Seahorse analyzer. The addition of CD155-Fc resulted in a significantly reduced OCR in human CD4⁺ T cells. Basal respiration, respiration coupled to ATP generation, maximal respiration, and spared respiratory capacity were decreased in human CD4⁺ T cells treated with CD155-Fc (Supplementary Fig. 12d, e). Consistently, ECAR was reduced in human CD4⁺ T cells stimulated with CD155-Fc (Supplementary Fig. 12f). These data indicate the important role of TIGIT in controlling glucose oxidation in both mouse and human CD4⁺ T cells.

The differentiation of CD4⁺ T cells is closely regulated by cellular metabolism, and glucose glycolysis is required for Th1 and Th17 cell differentiation³³. We thus hypothesized that TIGIT controls Th1 and Th17 cell differentiation by affecting glucose metabolism in CD4⁺ T cells. To test this hypothesis, we first excluded the involvement of fatty acid oxidation (FAO) and glutamine metabolism in TIGIT-mediated T-cell inhibition. *Tigit*^{−/−} CD4⁺ T cells were cultured under Th1- or Th17-polarizing conditions in the presence of the mitochondrial pyruvate carrier (MPC) inhibitors UK5099 and MSDC-0602 to block the transportation of pyruvate into mitochondria, the carnitine palmitoyltransferase 1a (CPT1a) inhibitor etomoxir (ETO) to inhibit FAO, and the glutaminase inhibitor bis-2-(5-phenylacetamido)-1, 2, 4-thiadiazol-2-yl ethyl sulfide (BPTES) to inhibit glutaminolysis (Fig. 6i), which did not affect cell viability (Supplementary Fig. 13). Our data revealed that the inhibition of MPC by either UK5099 or MSDC-0602 completely reversed the increase in T-bet and IFN γ expression in *Tigit*^{−/−} CD4⁺ T cells. Consistently, IL-17A⁺ cells were found to be expanded in *Tigit*^{−/−} CD4⁺ T cells, which was counteracted by the inhibition of MPC (Fig. 6i–k). However, inhibition of neither FAO nor glutaminolysis reversed the increased Th1 and Th17 differentiation in *Tigit*^{−/−} CD4⁺ T cells (Fig. 6i–k). These data suggest that TIGIT controls Th1 and Th17 cell differentiation through glucose metabolism in both human and mouse CD4⁺ T cells.

TIGIT controls Th1 and Th17 differentiation through metabolic-epigenetic reprogramming

Glucose-derived citrate in the TCA cycle can be used to supply cytosolic acetyl-CoA generation for histone acetylation. ATP-citrate lyase (ACLY) is responsible for cleaving citrate into acetyl-CoA in the cytosol³⁴ (Fig. 7a). A previous study showed that glycolysis promoted Th1 cell differentiation through an epigenetic mechanism¹⁶, linking glucose metabolism to CD4⁺ T-cell differentiation at the epigenetic level. We thus hypothesized that TIGIT controls acetyl-CoA generation in the cytosol in an ACLY-dependent manner. We first isolated CD4⁺ T cells from PM patients or HC and activated them with anti-CD3/CD28 beads for 3 d. Our data revealed that the expression of ACLY was notably greater in CD4⁺ T cells from patients with PM than in those



from HC (Fig. 7b). We then measured the amount of acetyl-CoA in the subcellular compartments of CD4⁺ T cells and found that the amount of acetyl-CoA was dramatically increased in CD4⁺ T cells from patients with PM. Most importantly, the amount of acetyl-CoA in the cytosol was significantly increased in CD4⁺ T cells from patients with PM. However, the amount of acetyl-CoA in the mitochondria of CD4⁺ T cells

did not differ between PM and HC (Fig. 7c). We used the MPC inhibitor UK5099 to further determine the contribution of glucose-derived citrate to the increase in cytosolic acetyl-CoA in CD4⁺ T cells from PM patients. The data revealed that UK5099 completely reversed the increased amount of acetyl-CoA in patient CD4⁺ T cells (Fig. 7c). These data indicate that the transportation of pyruvate into mitochondria is

Fig. 3 | Knockdown of TIGIT in healthy CD4⁺ T cells recapitulates the proinflammatory phenotype of PM TIGIT^{low} CD4⁺ T cells. **a, b** Knockdown of TIGIT was confirmed by flow cytometry. Data from five biologically independent replicates. **c** Knockdown of TIGIT in CD4⁺ T cells from HC or PM was confirmed by western blot. The experiment was repeated three times independently with similar results. **d–g** CD4⁺ T cells were labeled with CFSE and stimulated with α CD3/CD28 for 3 d. T-cell proliferation was evaluated by flow cytometry. Data from five biologically independent replicates. **h, i** IFN γ and IL-17A expression in CD4⁺ T cells was measured by flow cytometry. Data from five biologically independent replicates. **d–r** Naive CD4⁺ T cells from HC were stimulated by α CD3/CD28 for 1 d, and then transfected with scramble or TIGIT siRNA by electroporation. Following transfection, cells were subjected to culture conditions for Th1, Th2, Th17, and Treg cell

differentiation for an additional 4 d, respectively. **j–x** Naive CD4⁺ T cells from HC were stimulated by α CD3/CD28 for 1 d, and then transfected with scramble or TIGIT siRNA by electroporation. Following transfection, cells were subjected to culture conditions for Th1, Th2, Th17 and Treg cell differentiation for an additional 4 d, respectively. **j, k** Knockdown efficacy of TIGIT was confirmed by flow cytometry. Data from five biologically independent replicates. **l–x** Th1 condition: T-bet and IFN γ (**l–n**), Th2 condition: GATA3 and IL-4 (**o–r**), Th17 condition: ROR γ t and IL-17A (**s–v**), and Treg condition: FoxP3 (**w, x**) expression in CD4⁺ T cells were measured by flow cytometry. Representative contour plots or histograms were shown. Data from five biologically independent replicates. All data are mean \pm SEM. Statistics were done by a two-tailed unpaired Student's *t* test.

required for the increase in acetyl-CoA in the cytosol of CD4⁺ T cells from PM patients.

Acetyl-CoA impacts chromatin structure by providing acetyl groups for histone acetylation³⁵. We asked whether increased acetyl-CoA in the cytosol of CD4⁺ T cells from PM patients would lead to increased histone acetylation. Immunoblotting analysis revealed that histone acetylation on H3K27 and H3K9 was notably increased in CD4⁺ T cells from PM patients compared with those from HC (Fig. 7d). To functionally connect TIGIT to histone acetylation, we cultured CD4⁺ T cells from PM or HC with CD155-Fc. Our data revealed that the expression of ACLY and histone acetylation on H3K27 and H3K9 were dramatically reduced in HC CD4⁺ T cells cultured with CD155-Fc (Fig. 7e, f). However, TIGIT stimulation with CD155-Fc failed to reduce ACLY expression in CD4⁺ T cells from patients with PM. The acetylation of H3K27 and H2K9 in CD4⁺ T cells from PM patients was also not affected by TIGIT stimulation with CD155-Fc (Fig. 7e, f). Consistent with the data from patient cells, Tigit^{-/-} CD4⁺ T cells presented greater ACLY expression than did Tigit^{+/+} CD4⁺ T cells (Fig. 7g). Similarly, the amount of acetyl-CoA in the whole cell or cytosol was significantly increased in Tigit^{-/-} CD4⁺ T cells, which was reversed by MPC inhibition. Acetyl-CoA in mitochondria was observed to be similar between Tigit^{-/-} and Tigit^{+/+} CD4⁺ T cells (Fig. 7h). The increased acetyl-CoA in Tigit^{-/-} CD4⁺ T cells also led to increased acetylation of H3K27 and H3K9 (Fig. 7i). It has been shown that ACLY produces cytosolic acetyl-CoA and mediates de novo lipogenesis in B cells in response to LPS stimulation³⁶. However, we did not identify changed gene expression in the lipogenesis pathways in Tigit^{-/-} CD4⁺ T cells (Supplementary Fig. 14), suggesting that the increased acetyl-CoA is mainly used for histone modification.

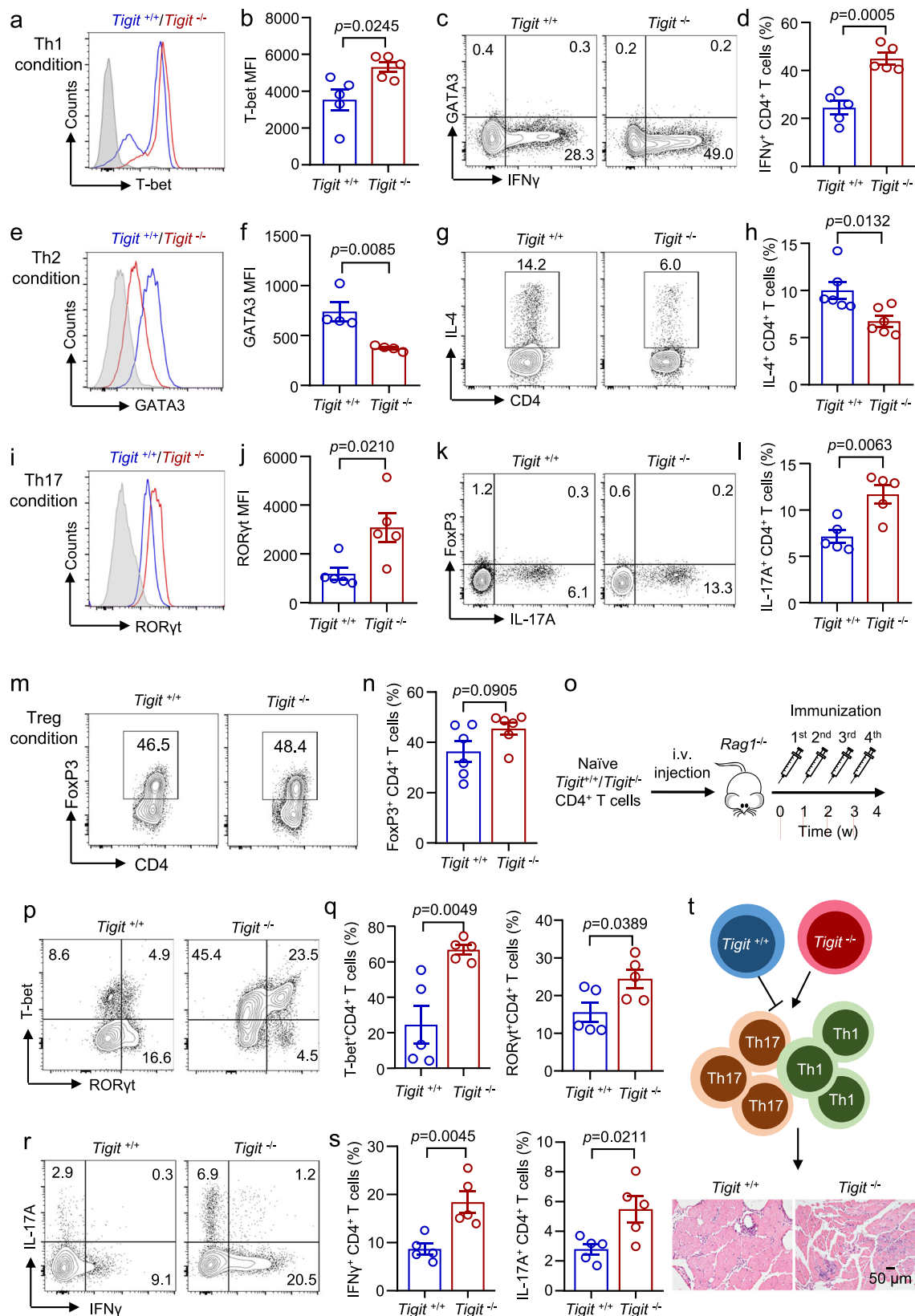
To further exclude the involvement of FAO and glutaminolysis as sources of acetyl-CoA in Tigit^{-/-} CD4⁺ T cells, CD4⁺ T cells were treated with the FAO inhibitor ETO, the glutaminolysis inhibitor BPTES, or the MPC inhibitor UK5099. Notably, the increased expression of ACLY in CD4⁺ T cells from PM patients was completely counteracted by treatment with the MPC inhibitor UK5099. Inhibition of FAO by ETO or inhibition of glutaminolysis by BPTES had no effect on ACLY expression in patient CD4⁺ T cells (Fig. 7j). Accordingly, enhanced acetylation of H3K27 and H3K9 in CD4⁺ T cells from PM patients was normalized by MPC inhibition. ETO and BPTES both failed to decrease the acetylation of H3K27 and H3K9 in CD4⁺ T cells from PM patients (Fig. 7k). Similar results were observed in Tigit^{-/-} CD4⁺ T cells (Fig. 7l, m). Another route for cytosolic acetyl-CoA generation is through the activity of acyl-CoA synthetase short-chain family members (ACSS)³⁷. To exclude the involvement of ACSS in elevated acetyl-CoA in Tigit^{-/-} or PM CD4⁺ T cells, the expression of ACSS1 and ACSS2 was measured by western blot. Neither ACSS1 nor ACSS2 expression was changed in Tigit^{-/-} or PM CD4⁺ T cells compared to Tigit^{+/+} or HC CD4⁺ T cells, respectively (Supplementary Fig. 15), suggesting that increased cytosolic acetyl-CoA in Tigit^{-/-} or PM CD4⁺ T cells is mainly due to ACLY-mediated cytosolic acetyl-CoA conversion. Here, we conclude that glucose-derived pyruvate is the major source of cytosolic acetyl-CoA generation for histone acetylation.

To dissect the impacts of TIGIT-mediated histone acetylation on CD4⁺ T-cell differentiation, we applied chromatin immunoprecipitation (ChIP) followed by qPCR to identify CD4⁺ T-cell differentiation-related genes that are associated with histone acetylation. ChIP-qPCR analysis revealed that knockout of TIGIT resulted in increased H3K9 acetylation at the *ifng* promoter and the CNS22 region. Moreover, the acetylation of H3K27 at the *Il17* promoter, CNS2, and CNS22 regions was also increased in Tigit^{-/-} CD4⁺ T cells. Although the difference did not reach statistical significance, a strong increasing trend was observed in H3K27 acetylation at the *ifng* promoter region in Tigit^{-/-} CD4⁺ T cells (Fig. 7n). To study the underlying mechanism of the inhibitory effects of TIGIT on Th1 and Th17 cell differentiation, naive Tigit^{-/-} or Tigit^{+/+} CD4⁺ T cells were polarized under Th1 and Th17 conditions in the presence of the histone acetylation inhibitor C646. No cytotoxicity was observed in T cells exposed to either low (1 μ M) or high concentrations (5 μ M) of C646 (Supplementary Fig. 16a–d). We observed that Tigit^{-/-} CD4⁺ T cells were more sensitive to the inhibition of histone acetylation by C646 than were Tigit^{+/+} CD4⁺ T cells. A low concentration of C646 decreased the percentages of T-bet⁺ and IFN γ ⁺ CD4⁺ T cells among Tigit^{-/-} CD4⁺ T cells under Th1-polarizing conditions (Fig. 7o–q, Supplementary Fig. 16e, f). Similarly, the percentages of ROR γ t⁺ and IL-17A⁺ CD4⁺ T cells were reduced in Tigit^{-/-} CD4⁺ T cells under Th17-polarizing conditions by 1 μ M C646 (Fig. 7r–t, Supplementary Fig. 16g, h). Although a high concentration (5 μ M) of C646 was able to suppress the differentiation of IFN γ ⁺ Th1 cells and IL-17A⁺ Th17 cells, a low concentration (1 μ M) of C646 had no effect on Th1 and Th17 cell differentiation from naive Tigit^{+/+} CD4⁺ T cells (Fig. 7o–t, Supplementary Fig. 16). We further investigated the regulation of histone acetylation during the differentiation of human CD4⁺ T cells. We found that 1 μ M C646 effectively reduced the percentage of T-bet⁺IFN γ ⁺ Th1 cells when differentiated from patient naive CD4⁺ T cells (Supplementary Fig. 17a, b). Similarly, the percentage of IL-17A⁺ Th17 cells was profoundly decreased by 1 μ M C646 when these cells were differentiated from patient naive CD4⁺ T cells (Supplementary Fig. 17c, d). Consistently, 1 μ M C646 was not able to suppress the differentiation of Th1 and Th17 cells from HC naive CD4⁺ T cells (Supplementary Fig. 17). These data suggest that TIGIT-deficient CD4⁺ T cells are more sensitive to the inhibition of histone acetylation, revealing that histone acetylation is the major downstream target of TIGIT in CD4⁺ T cells.

Together, these data indicate that TIGIT controls Th1 and Th17 cell differentiation by increasing glucose-derived acetyl-CoA generation for histone acetylation.

TIGIT controls Th1 and Th17 cell differentiation through histone acetylation in autoimmune myositis

To further address whether TIGIT-controlled Th1 and Th17 cell differentiation is histone acetylation-dependent in vivo, we treated EAM mice with the histone acetylation inhibitor C646. Mice treated with C646 presented reduced T-bet and ROR γ t expression in CD4⁺ T cells. The production of IL-17A and IFN γ was profoundly reduced by C646 treatment, resulting in decreased inflammatory infiltrates in the muscle (Supplementary Fig. 18). Next, naive CD4⁺ T cells from



Tbet^{-/-} or *Tbet*^{+/+} mice were injected into *Rag1*^{-/-} mice. The mice were challenged with autologous myosin and treated with C646 or vehicle (Fig. 8a). In mice that received *Tbet*^{-/-} T cells, the expression of Tbet and RORyt was significantly greater than that in mice that received *Tbet*^{+/+} T cells, which was completely reversed by C646 treatment (Fig. 8b–d). Similarly, the percentages of IL-17A⁺ and

IFN γ ⁺ CD4⁺ T cells were notably higher in the mice that received *Tbet*^{-/-} T cells than in the mice that received *Tbet*^{+/+} T cells. Consistently, C646 decreased the percentages of IL-17A⁺ and IFN γ ⁺ CD4⁺ T cells in mice that received *Tbet*^{-/-} T cells to the same level as those in mice that received *Tbet*^{+/+} T cells (Fig. 8e, f). We did not observe a difference in FoxP3-expressing CD4⁺ T cells between mice receiving

Fig. 4 | TIGIT controls the differentiation of Th1 and Th17 cells in vitro and in vivo. a–n Naive CD4⁺ T cells were isolated from *Tigit*^{−/−} or *Tigit*^{+/+} mice. The cells were subjected to culture conditions for Th1, Th2, Th17 and Treg cell differentiation for 5 d. **a–d** Th1 condition: T-bet, GATA3, and IFN γ expression in CD4⁺ T cells was measured by flow cytometry, and representative contour plots were shown. **e–h** Th2 condition: flow cytometric analysis of GATA3 and IL-4 expression in CD4⁺ T cells and representative contour plots. **i–l** Th17 condition: ROR γ t and IL-17A expression in CD4⁺ T cells measured by flow cytometry. **m, n** Treg condition: FoxP3 expression in CD4⁺ T cells measured by flow cytometry and representative contour plots. **o** Scheme of the mouse experiment. EAM was induced as described in Fig. 2.

Each *Rag1*^{−/−} recipient mouse was injected intravenously with 2×10^6 naive CD4⁺ T cells, and EAM induction was performed. **p–s** The expression of T-bet, ROR γ t, IFN γ , and IL-17A in CD4⁺ T cells from mice that received *Tigit*^{−/−} or *Tigit*^{+/+} cells was measured via flow cytometry. Representative contour plots were shown. **t** Schematic employed to visualize that TIGIT deficiency enhances Th1 and Th17 differentiation, resulting in severe muscle infiltration. Original magnification: $\times 200$. **b, d, j, l, q, s**, $n = 5$; for **f**, $n = 4$; and for **h**, $n = 6$ biological independent samples. All data are presented as the mean \pm SEM. Statistics were done by two-tailed unpaired Student's *t* test.

Tigit^{−/−} or *Tigit*^{+/+} T cells. C646 treatment had no effect on the expression of FoxP3 in *Tigit*^{−/−} T cells (Fig. 8g, h).

A humanized mouse model was adopted to determine whether histone acetylation is required for the differentiation of CD4⁺ T cells from PM patients in vivo. PBMCs from PM patients or HC were adoptively transferred into immune-deficient NCG mice. Alternatively, NCG mice that received patient PBMCs were treated with C646 (Fig. 8i). Mice that received patient PBMCs had more severe disease than did mice that received HC PBMCs. Muscle strength was weaker in the mice that received patient PBMCs. C646 treatment increased muscle strength in mice that received patient PBMCs in the control group (Fig. 8j). Tissue infiltration was also more intense in the mice that received patient PBMCs, which was completely reversed by C646 treatment (Fig. 8k). The spleen weight index of the mice that received patient PBMCs was 2.1 times higher than that of the mice that received HC PBMCs (Fig. 8l, m). The percentages of IFN γ ⁺ and IL-17A⁺ CD4⁺ T cells in the spleen were significantly expanded in mice that received patient PBMCs, and the percentages of IFN γ ⁺ and IL-17A⁺ CD4⁺ T cells were 1.7 and 4.6 times greater than those in HC PBMCs, respectively (Fig. 8n, o). Consistently, C646 treatment profoundly reduced the proinflammatory CD4⁺ T-cell response in mice that received patient PBMCs to levels similar to those in mice that received HC PBMCs (Fig. 8l–o).

TIGIT impairs CD28 signaling and inhibits CD4⁺ T-cell responses

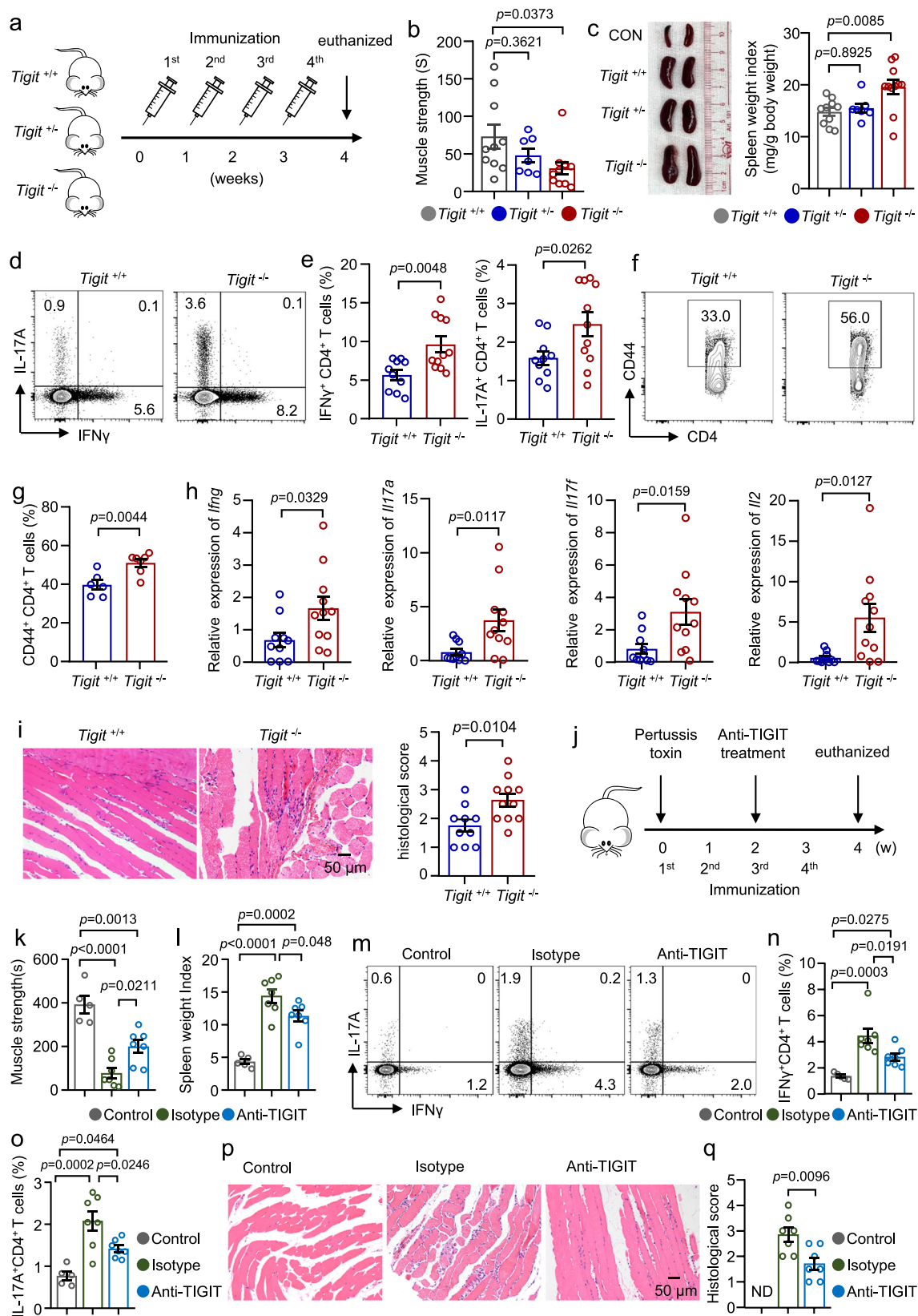
The activation of T cells relies on TCR stimulation and costimulatory signaling through CD28³⁸. TIGIT acts as an inhibitory molecule that competes with CD226 for its common ligand CD155²⁷. To determine the underlying signaling pathways by which TIGIT inhibits T-cell responses, *Tigit*^{−/−} or *Tigit*^{+/+} CD4⁺ T cells were isolated and activated with anti-CD3/CD28 beads. Our data revealed that knockout of TIGIT did not affect the phosphorylation of CD226. The level of phosphorylated CD226 was similar between *Tigit*^{−/−} and *Tigit*^{+/+} CD4⁺ T cells (Fig. 9a, b). Since CD4⁺ T cells from PM patients were deficient in TIGIT expression, the phosphorylation of CD226 was further assessed in CD4⁺ T cells from patients with PM. We did not observe differences in the phosphorylation of CD226 between CD4⁺ T cells from PM patients and those from HC (Fig. 9b). Next, we validated whether TIGIT exerts direct effects on TCR signaling. The phosphorylation of ZAP70 and LCK in the TCR signaling pathway was notably induced by TCR stimulation via OKT3. However, the phosphorylation of ZAP70 and LCK did not differ between *Tigit*^{−/−} and *Tigit*^{+/+} CD4⁺ T cells (Fig. 9c), suggesting that TCR signaling is not altered by TIGIT knockout. To determine whether TIGIT affects TCR signaling in human cells, we stimulated CD4⁺ T cells from HC with OKT3 in combination with or without CD155-Fc. We found that the phosphorylation of ZAP70 and LCK did not change when CD4⁺ T cells were stimulated with additional CD155-Fc (Fig. 9d). TCR signaling was not altered in CD4⁺ T cells from PM patients or HC, and the phosphorylation of ZAP70 and LCK was similar (Fig. 9e). TCR-mediated calcium influx was also not different between *Tigit*^{−/−} and *Tigit*^{+/+} CD4⁺ T cells (Fig. 9f). CD28 activates the PI3K-AKT-mTOR pathway and provides strong costimulatory signaling for T-cell activation^{39,40}. Our data revealed that the phosphorylation of PI3K, AKT, and S6 was significantly increased in *Tigit*^{−/−} CD4⁺ T cells after anti-CD3/CD28 stimulation (Fig. 9g). Moreover, the

phosphorylation of mTOR and Raptor expression were both notably increased in *Tigit*^{−/−} CD4⁺ T cells after anti-CD3/CD28 stimulation (Fig. 9h). Consistently, overexpression of TIGIT reduced the phosphorylation of AKT and S6 in CD4⁺ T cells from both PM and HC. The phosphorylation of AKT and S6 was increased in CD4⁺ T cells from PM, which was counteracted when TIGIT expression in patient CD4⁺ T cells was rescued (Supplementary Fig. 19). These data suggest that TIGIT inhibits T-cell activation by downregulating the CD28-mediated PI3K-AKT-mTOR pathway. We speculated that TCR signaling is not involved in TIGIT-mediated T-cell suppression.

To determine whether CD28 signaling serves as a downstream target of TIGIT, we bypassed the TCR by stimulating CD4⁺ T cells with PMA plus anti-CD28. Our data revealed that the proliferation and levels of the activation markers CD44 and CD69 were significantly higher in *Tigit*^{−/−} CD4⁺ T cells than in *Tigit*^{+/+} CD4⁺ T cells when stimulated with anti-CD28 plus PMA (Fig. 9i–m). We then tested whether the inhibition of CD28 signaling by PI3K inhibitor BEZ235 or PI-103 was able to reverse T-cell activation in *Tigit*^{−/−} CD4⁺ T cells. BEZ235 was titrated to low concentrations (0.1 μ M) and high concentrations (1 μ M). We observed that 0.1 μ M BEZ235 was able to inhibit proliferation and decrease CD44 and CD69 expression in *Tigit*^{−/−} CD4⁺ T cells to a level similar to that of *Tigit*^{+/+} CD4⁺ T cells without affecting cell viability (Fig. 9i–m, Supplementary Fig. 20a, b). Anti-CD28 plus PMA stimulation biased *Tigit*^{−/−} CD4⁺ T cells into IFN γ - and IL-17A-producing cells under polarizing conditions. Notably, 0.1 μ M BEZ235 not only decreased the expression of T-bet and IFN γ in *Tigit*^{−/−} CD4⁺ T cells but also reduced the expression of ROR γ t and IL-17A in *Tigit*^{−/−} CD4⁺ T cells. Although a relatively high concentration (1 μ M) of BEZ235 was able to inhibit Th1 and Th17 cell differentiation from naive *Tigit*^{+/+} CD4⁺ T cells, 0.1 μ M BEZ235 had no effect on Th1 and Th17 cell differentiation from naive *Tigit*^{+/+} CD4⁺ T cells (Fig. 9n–s, Supplementary Fig. 20c–j). Similar results were found when using another PI3K inhibitor PI-103 (Fig. 9i–s, Supplementary Fig. 21). Together, these data suggest that TIGIT dampens CD28 signaling in CD4⁺ T cells and suppresses the differentiation of Th1 and Th17 cells.

TCR signaling is not involved with TIGIT-mediated T-cell inhibition

To further exclude the involvement of TCR in TIGIT-mediated T-cell suppression, the TCR downstream signaling NF- κ B was further investigated, finding out that NF- κ B signaling was not different between *Tigit*^{−/−} and *Tigit*^{+/+} CD4⁺ T cells as quantified by western blot (Fig. 10a). We then used PHA, which binds to TCR/CD3 complex to activate CD4⁺ T cells, mimicking the intracellular activation events triggered by anti-CD3 antibodies⁴¹. In addition, phorbol-12-myristate-13-acetate (PMA) can bypass TCR to activate T cells through protein kinase C⁴². As expected, we did not observe differences in the expression of CD44, CD69, or CD25 in *Tigit*^{−/−} CD4⁺ T cells when stimulated with PMA in combination with PHA. T-cell proliferation was also not different between *Tigit*^{−/−} and *Tigit*^{+/+} CD4⁺ T cells when stimulated with PMA in combination with PHA. Similar results were found when CD4⁺ T cells were stimulated with OKT3 in combination with PMA (Fig. 10b–e). We further stimulated cells with anti-CD3 or anti-CD3/anti-CD28. Proliferation assay revealed that TIGIT does not significantly impact T-cell



proliferation under anti-CD3 stimulation (Fig. 10f–h). Consistently, IL-2 production was similar between *Tigrit*^{-/-} and *Tigrit*^{+/+} CD4⁺ T cells when stimulated with anti-CD3 alone, while *Tigrit*^{-/-} CD4⁺ T cells showed enhanced IL-2 production when stimulated with anti-CD3/anti-CD28 (Fig. 10i, j), excluding the involvement of TCR signaling in TIGIT-mediated T-cell inhibition.

Discussion

Aberrant activation of autoreactive T cells with inflammatory infiltration in the muscle is the hallmark of patients with PM². It has been shown that Th1 and Th17 cells are notably expanded in the peripheral blood of patients with PM. The IFN γ and IL-17A signatures are both enriched in inflamed tissue in PM patients⁴³. TIGIT is an important

Fig. 5 | Knockout of TIGIT promotes inflammatory CD4⁺ T-cell responses during EAM induction. **a** Scheme for the induction of experimental autoimmune myositis (EAM) in *Tigit*^{-/-}, *Tigit*^{+/-}, or *Tigit*^{+/+} mice. Age- and sex-matched *Tigit*^{+/+} mice without EAM induction served as the Control group. **b** Muscle strength of *Tigit*^{-/-}, *Tigit*^{+/-}, or *Tigit*^{+/+} mice with EAM. **c** Representative spleen images and the spleen weight index calculated by dividing the spleen weight (mg) by the body weight (g). **d, e** IFN γ - and IL-17A-producing CD4⁺ T cells in the spleens of *Tigit*^{-/-} or *Tigit*^{+/+} mice were measured by flow cytometry. Representative contour plots were shown (**f, g**) CD44 expression in CD4⁺ T cells in the spleens of *Tigit*^{-/-} or *Tigit*^{+/+} mice was measured by flow cytometry. **h** Gene expression of *Irfng*, *Il17a*, *Il17f*, and *Il2* in the quadriceps of *Tigit*^{-/-} or *Tigit*^{+/+} mice was quantified by qPCR. **i** HE staining and histological score of quadriceps in *Tigit*^{-/-} or *Tigit*^{+/+} mice with EAM. Original magnification: $\times 200$. **j, k** TIGIT agonistic antibody (Anti-TIGIT) or an isotype control was used to treat EAM mice. **j** EAM was induced as described in **a**. EAM mice were injected intra-peritoneally with anti-TIGIT (10 mg/kg/Q3d) or an isotype after the second

immunization for 2 weeks (w). Age- and sex-matched C57BL/6 mice without EAM induction served as the Control group. **k** Muscle strength of the control mice and mice with EAM treated with anti-TIGIT or the isotype control. **l** Size of spleen and spleen weight. Spleen weight index was calculated and summarized in **c**. **m–o** IFN γ - and IL-17A-producing CD4⁺ T cells in the spleen were measured by flow cytometry. **p, q** HE staining and histological score of quadriceps sections from control mice and mice with EAM treated with anti-TIGIT or the isotype control. Original magnification: $\times 200$. ND: not detectable. **b, c, e, h, i** *Tigit*^{-/-} ($n = 11$), *Tigit*^{+/-} ($n = 7$), and *Tigit*^{+/+} ($n = 10$) biologically independent replicates, when applicable. **g** *Tigit*^{-/-} ($n = 7$), and *Tigit*^{+/+} ($n = 6$) biologically independent replicates. **k, l, n, o, q** Control ($n = 5$), Isotype ($n = 7$), and Anti-TIGIT ($n = 7$) biological independent samples, when applicable. All data are presented as the mean \pm SEM. Statistics were done by one-way ANOVA with adjustments for multiple comparisons in **b, c, k, l, n, o**, and two-tailed unpaired Student's *t* test in **e, g, h, i, q**.

inhibitory receptor that contributes to immune tolerance²⁷. Here, our data revealed that TIGIT is deficient in CD4⁺ T cells from patients with PM. As a result, the engagement of TIGIT by CD155 failed to suppress IFN γ and IL-17A production by CD4⁺ T cells from PM patients. TIGIT deficiency promoted glucose oxidation and pyruvate flux-dependent cytosolic acetyl-CoA generation and histone acetylation, which biased CD4⁺ T cells to differentiate into Th1 and Th17 cells. Our study provides evidence that cell-intrinsic TIGIT controls the differentiation of Th1 and Th17 cells through a metabolic-epigenetic mechanism, and TIGIT deficiency could contribute to the pathogenesis of PM.

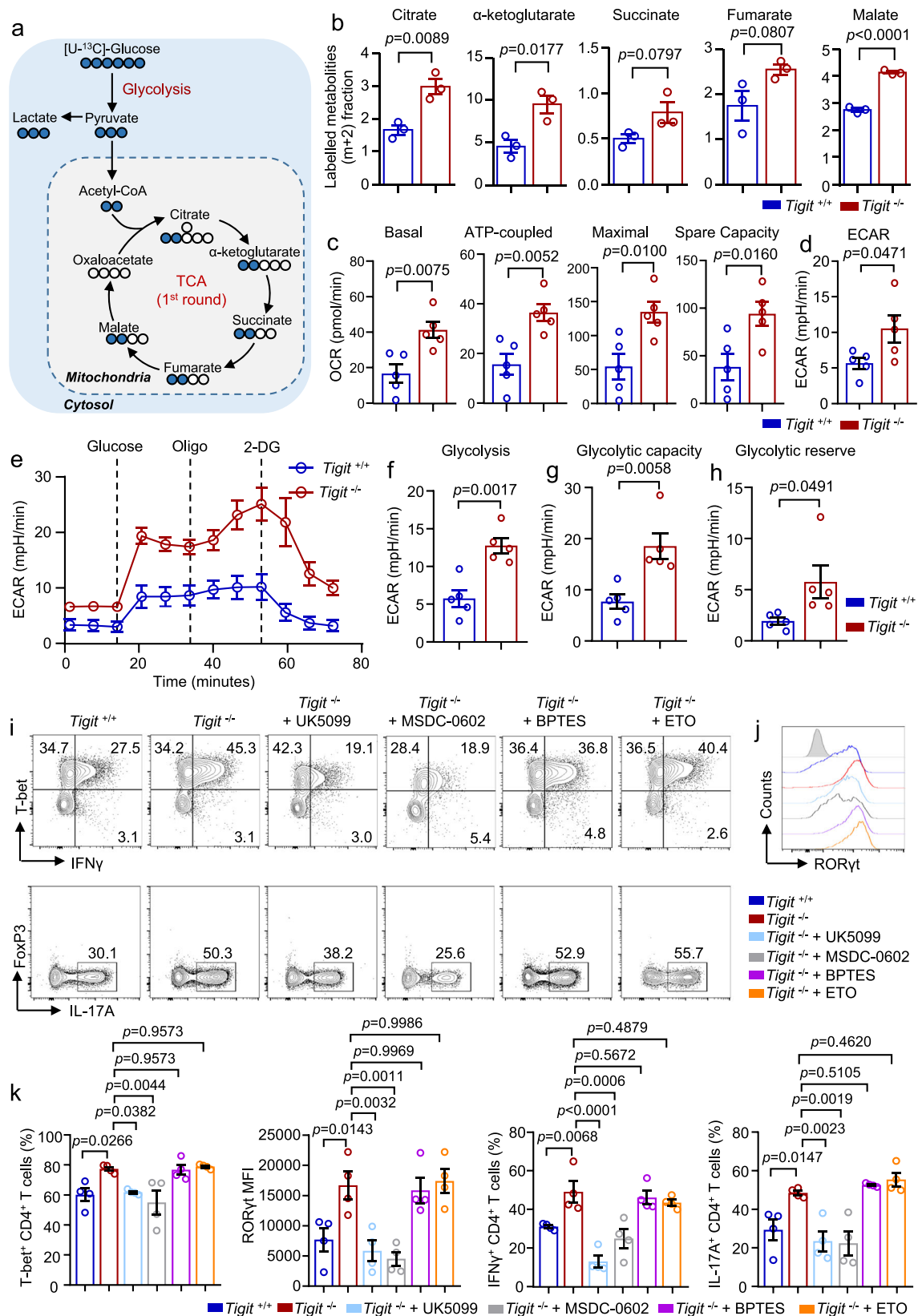
In autoimmunity, CD4⁺ T cells are found to exhibit pronounced co-stimulation signals⁴⁴. TIGIT represents an important immune checkpoint that plays an essential role in maintaining immune tolerance and preventing autoimmunity^{27,45}. It has been shown that TIGIT expression in CD4⁺ T cells was lower in the synovial fluid of patients with active rheumatoid arthritis (RA), and overexpression of TIGIT decreased the production of IFN γ and IL-17 by RA CD4⁺ T cells⁴⁶. Although TIGIT expression on CD4⁺ T cells was increased in patients with SLE, the administration of CD155 or TIGIT-Fc suppressed CD4⁺ T cells and reduced disease development in lupus mice^{30,47}. Consistent with a previous report⁴⁸, our data revealed that TIGIT expression was impaired in CD4⁺ T cells from patients with PM. We further showed that TIGIT expression was specifically reduced in IFN γ - and IL-17A-producing CD4⁺ T cells in PM patients. Cell-intrinsic deficiency of TIGIT could lead to hyper-responses of Th1 and Th17 cells in patients with PM, suggesting the involvement of TIGIT deficiency in the development and progression of myositis. For defects in TIGIT expression, CD155-Fc failed to suppress IFN γ and IL-17A production by CD4⁺ T cells from PM patients. Interestingly, overexpression of TIGIT in CD4⁺ T cells from PM patients was able to suppress the inflammatory phenotype of patient CD4⁺ T cells. Compared with those in wild-type mice, Th1 and Th17 responses were enhanced, and muscle inflammation was increased in EAM mice, highlighting the role of TIGIT in preventing autoreactive T-cell responses and the development of autoimmune myositis.

Studies have focused on understanding the regulatory effect of TIGIT on CD8⁺ T-cell exhaustion in cancers^{27,49,50}. The functions of TIGIT and the underlying mechanisms in CD4⁺ T cells are less clear. Extrinsically, TIGIT can suppress T-cell activation by promoting the generation of tolerogenic DCs²². In addition, TIGIT can promote its inhibitory effects by enhancing Treg functions²⁸. Impaired TIGIT expression on B cells could promote Tfh cell expansion in multiple sclerosis⁵¹. Interestingly, TIGIT can inhibit T-cell activation in a cell-intrinsic manner^{25,26}. Cell-intrinsic TIGIT signaling reduces the production of the proinflammatory cytokines IFN γ and IL-17A by CD4⁺ T cells and potentially prevents the development of autoimmune diseases in mouse models^{26,52,53}. However, the function of TIGIT in CD4⁺ T-cell differentiation has not been studied. By using *Tigit*^{-/-} and *Tigit*^{+/+} CD4⁺ T cells, we provide strong evidence that Th1 and Th17 cell differentiation from naive CD4⁺ T cells was enhanced when TIGIT was

knocked out in vitro. In addition to the cytokines IFN γ and IL-17A, which were profoundly increased in *Tigit*^{-/-} CD4⁺ T cells, the master transcription factors T-bet and ROR γ t for Th1 and Th17 cells, respectively, were both significantly increased. The knockout of TIGIT had no effect on the differentiation of Treg cells. By transferring naive *Tigit*^{-/-} and *Tigit*^{+/+} CD4⁺ T cells into *Rag1*^{-/-} mice, we demonstrated that the differentiation of Th1 and Th17 cells was notably increased in mice that received TIGIT-deficient CD4⁺ T cells, resulting in more severe autoimmune myositis. The percentage of Treg cells was unaffected. In Treg cells, TIGIT induces the suppressive mediator Fgl2 to impose a stronger inhibitory effect on TIGIT⁺ Treg cells than TIGIT⁻ Treg cells do²⁸. Knockout of TIGIT might also impair Treg cell function. Nevertheless, we provide direct evidence that TIGIT controls CD4⁺ T-cell differentiation and that knockout of TIGIT unleashes type 1 and type 17 proinflammatory responses during autoimmune myositis induction.

Cellular metabolism is profoundly reprogrammed during CD4⁺ T-cell differentiation, and glucose glycolysis is required for the differentiation of Th1 and Th17 cells^{14,54}. Both co-stimulatory and co-inhibitory molecules have been linked to cellular metabolism to control T-cell fate^{39,55}. CD28-mediated glycolysis is essential for T-cell activation and proliferation⁵⁶. PD-1 inhibits glycolysis and promotes lipolysis and FAO in T cells⁵⁷. In the tumor setting, TIGIT suppresses glucose glycolysis in CD8⁺ T cells and impairs their antitumor response⁵⁸. However, whether TIGIT plays a role in CD4⁺ T-cell metabolism is unknown. Here, we report that both patient TIGIT^{low} and *Tigit*^{-/-} CD4⁺ T cells demonstrated enhanced glucose metabolism. In normal mouse CD4⁺ T cells, mitochondrial oxygen consumption was increased during activation and differentiation when TIGIT was ablated. In addition, TIGIT engagement by CD155 resulted in reduced mitochondrial oxidation in human CD4⁺ T cells. [¹³C]-Glucose isotope tracing provided direct evidence that the ablation of TIGIT not only promoted glycolytic influx but also promoted the transportation of pyruvate into mitochondria to fuel the TCA cycle. Targeting mitochondrial respiration was sufficient to inhibit Th1 and Th17 cell responses and suppress autoimmunity^{59–61}. The data presented here predict that TIGIT deficiency rewrites glucose metabolism in CD4⁺ T cells and biases them toward proinflammatory Th1 and Th17 cells in patients with PM.

Recent findings support the concept that metabolites are not only substrates for energy generation but also directly or indirectly involved in T-cell differentiation through epigenetic remodeling of T cells^{20,54}. Acetyl-CoA is the central metabolite produced in the cytosol by ACLY using mitochondria-TCA cycle-derived citrate. Acetyl-CoA provides acetyl groups for histone acetylation to drive the epigenetic control of gene expression³⁴. In Th1 cells, deletion of lactate dehydrogenase A decreased the cytosolic acetyl-CoA level and inhibited histone acetylation¹⁶. The glucose transporter GLUT3 controlled Th17 cell responses through ACLY-dependent acetyl-CoA generation and histone acetylation¹⁷. In RA patients, SUCLG2 deficiency led to the



accumulation of α-ketoglutarate, citrate, and acetyl-CoA in CD4⁺ T cells, resulting in the generation of tissue-invasive CD4⁺ T cells⁶². In line with these studies, the data reported here revealed that increased levels of acetyl-CoA in patient TIGIT^{low} and *Tig1t*^{-/-} CD4⁺ T cells led to increased H3K9 and H3K27 acetylation in these TIGIT-deficient CD4⁺ T cells. Importantly, the inhibition of pyruvate transport into

mitochondria completely abrogated the increase in acetyl-CoA levels and histone acetylation in TIGIT-deficient T cells, indicating the essential role of glycolysis-derived pyruvate in TIGIT-controlled acetyl-CoA generation and histone modification. Recently, data have shown that MPC ablation or inhibition does not affect epigenome remodeling or the effector function of CD4⁺ T cells⁶³. Our data clearly showed that

Fig. 6 | TIGIT deficiency fuels glucose oxidation to promote Th1 and Th17 cell differentiation. **a** Isotope tracing of glucose-derived metabolites via GC/MS or LC/MS. **b** Fractional enrichment of [^{13}C]-glucose-derived metabolites in tricarboxylic acid (TCA) cycle in *Tigit*^{-/-} or *Tigit*^{+/+} CD4⁺ T cells. Data from three biologically independent replicates. **c, d** *Tigit*^{-/-} or *Tigit*^{+/+} CD4⁺ T cells were activated with $\alpha\text{CD3/CD28}$ for 3 d. Oxygen consumption rate (OCR) and basal extracellular acidification rate (ECAR) were measured using a Seahorse XF96 analyzer. Parameters of basal respiration, respiration coupled to ATP production, maximal respiration, respiratory spare capacity, and basal ECAR were summarized and data from five biologically independent replicates. **e–h** For metabolic activities evaluation of CD4⁺ T cells, Glycolysis Stress Test Kit was used to test ECAR by a Seahorse XF96 analyzer. ECAR tracing

curves and parameters of glycolysis, glycolysis capacity, and glycolysis reserve were summarized ($n =$ five biologically independent replicates from five individual mice per group). **i–k** Naive *Tigit*^{-/-} or *Tigit*^{+/+} CD4⁺ T cells were cultured under Th1- or Th17-polarizing condition for 5 d. UK5099 (20 μM), MSDC-0602 (10 μM), Etomoxir (ETO, 1 μM), or bis-2-(5-phenylacetamido-1, 2, 4-thiadiazol-2-yl) ethyl sulfide (BPTES, 3 μM) was included for the last 48 h of culture. IFN γ , T-bet, IL-17A, and ROR γt expression in CD4⁺ T cells were measured by flow cytometry. Data from four biologically independent replicates. All data are presented as the mean \pm SEM. Statistics were done by two-tailed unpaired Student's t test in (**b–d**, **f–h**) or one-way ANOVA followed by adjustments for multiple comparisons in **k**.

MPC inhibition led to significantly reduced cytosolic acetyl-CoA generation, histone acetylation, and CD4⁺ T-cell function in patient TIGIT^{low} and mouse *Tigit*^{-/-} CD4⁺ T cells. We speculate that enhanced glucose metabolism and pyruvate transportation into mitochondria in these TIGIT-deficient T cells represent the major source for citrate generation, which could promote cytosolic acetyl-CoA generation. In addition, the TPM value of MPC2 in CD4⁺ T cells is similar to that of MPC1 (The Human Protein Atlas). The use of MPC1-flox mice in the present study might have led to incomplete ablation of MPC activity⁶³.

TIGIT contains an immunoreceptor tyrosine-based ITIM and an ITT-like motif that is important for its inhibitory effects. Early studies using NK cell lines revealed that the binding of Grb2 and β -arrestin led to Fyn- and Lck-mediated phosphorylation of tyrosine residues in both motifs. SHIP1 was then recruited and interfered with downstream activation signals^{24,64}. More recently, data have shown that the inhibitory potential of TIGIT might rely more on the ITT-like domain than the ITIM in a modified human T-cell line⁶⁵. How primary CD4⁺ T cells are affected by cell-intrinsic TIGIT inhibitory signals remains elusive. TIGIT actively competes with CD226 for its common ligands⁵². TIGIT can directly bind to CD226 in cis and impair the costimulatory signal⁵⁰. TIGIT can also inhibit the phosphorylation of CD226 and thus impair its costimulation in CD8⁺ T cells in cancer²⁹. However, we observed similar phosphorylation levels of CD226 between *Tigit*^{-/-} and *Tigit*^{+/+} CD4⁺ T cells in this study. The phosphorylation of CD226 was also not altered in patient TIGIT^{low} CD4⁺ T cells. Moreover, we observed a low frequency of CD226 and TIGIT coexpression in both patient and HC CD4⁺ T cells (Supplementary Fig. 22), making CD226 unlikely to be affected by TIGIT. These data are in line with a recent study showing that TIGIT directly inhibited lymphocyte activation independent of CD226⁶⁵.

Microarray analysis revealed that TIGIT can act directly on T cells by attenuating TCR-driven activation signals²⁶. Like PD-1 and CD28, TIGIT clusters colocalized within nanometers of TCR clusters upon binding. However, no reduction in the phosphorylation of CD3 ζ , Zap70, or LAT was observed when TIGIT was proximate to TCR⁶⁵, suggesting that TIGIT does not reduce TCR signaling during activation. Similarly, TCR signaling was not altered when TIGIT was knocked out in CD4⁺ T cells. We observed similar levels of phosphorylated ZAP70 and LCK in *Tigit*^{-/-} and *Tigit*^{+/+} CD4⁺ T cells after TCR stimulation. The phosphorylation of ZAP70 and LCK was also not different between the TIGIT^{low} CD4⁺ T cells of PM patients and those of HC. Here, we provide direct evidence that TIGIT deficiency has no effect on TCR signaling in either primary human or mouse CD4⁺ T cells. We further excluded the involvement of TCR in TIGIT-mediated T-cell inhibition, as OKT3 or PHA stimulation had no effect on T-cell activation or proliferation. In contrast, stimulation of CD4⁺ T cells by PMA and an anti-CD28 antibody bypassing TCR led to enhanced T-cell activation and Th1/Th17 differentiation in *Tigit*^{-/-} CD4⁺ T cells, which was counteracted when CD28 signaling was inhibited. CD28 costimulation, which acts through PI3K and AKT, is required for T cells to increase glycolysis in response to activation⁵⁶. Our previous study revealed that CD28 blockade reduced glucose metabolism and autoreactive CD4⁺ T cells in vasculitis⁶⁶. Together, TIGIT impairs CD28 signaling and controls autoimmune-associated glucose metabolism in CD4⁺ T cells.

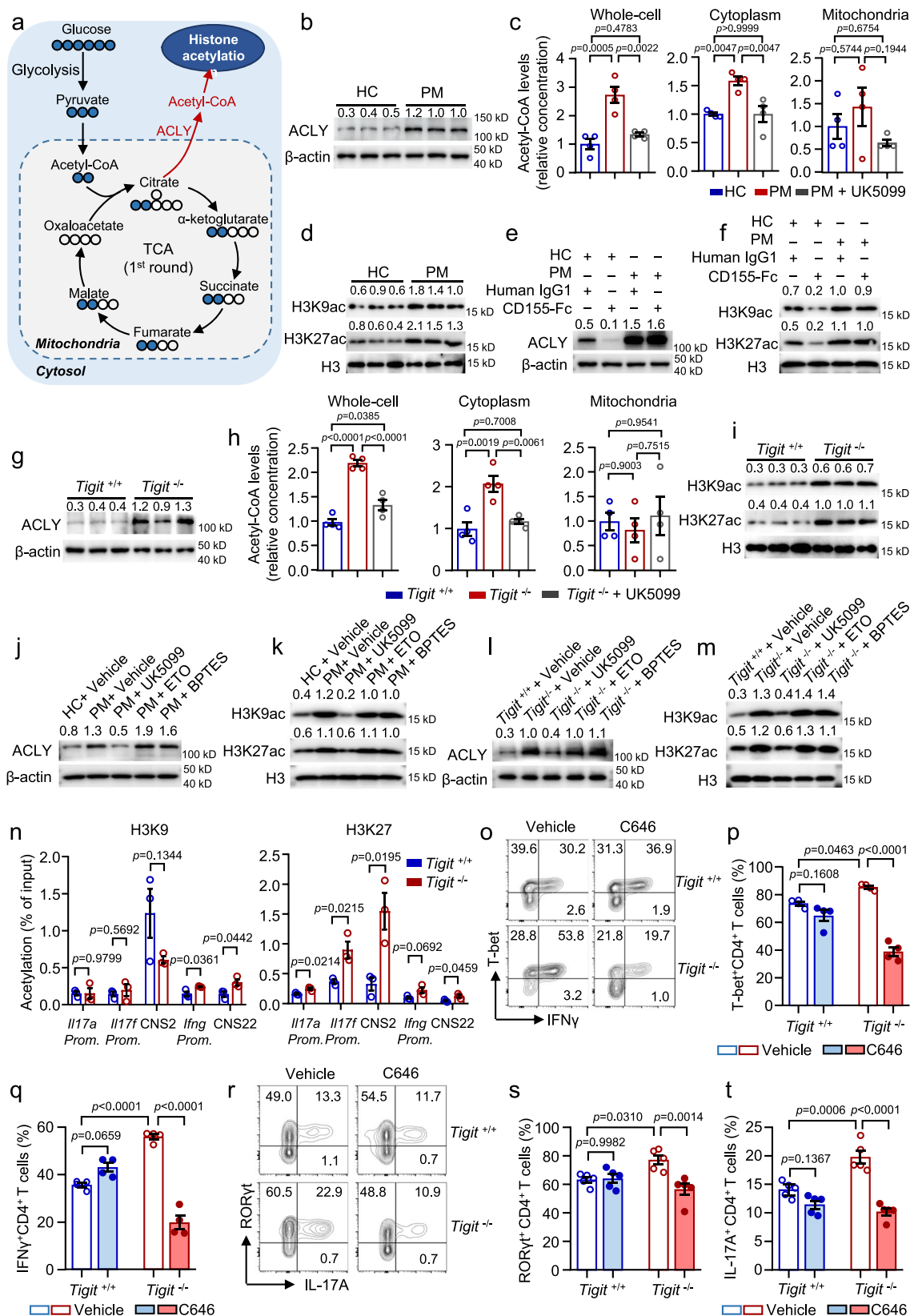
While all PM patients in this study were recruited according to standardized criteria (2017 European League Against Rheumatism/American College of Rheumatology Classification Criteria (EULAR/ACR) classification criteria for adult idiopathic inflammatory myopathies), it should be noted that PM encompasses distinct clinical subsets including anti-synthetase syndrome, inclusion body myositis, and immune-mediated necrotizing myopathy, each characterized by unique myositis-specific antibodies and pathogenic mechanisms. Given this marked clinical and pathophysiological heterogeneity among PM subgroups, the current findings may have less generalizability to specific disease subtypes and require cautious interpretation in subtype-specific contexts. In addition, the EAM model demonstrates substantial face validity through its recapitulation of key PM features, including characteristic inflammatory muscle infiltration patterns, muscle fiber atrophy, and enhanced CD4⁺ T-cell accumulation in perimysial and perivascular regions⁶⁷. This model provides a valuable platform for investigating immune-mediated mechanisms in myositis pathogenesis. However, it is important to acknowledge that the EAM paradigm does not fully replicate the complex clinical-pathological spectrum of human PM. Consequently, the mechanistic insights derived from this model may not comprehensively reflect the multifaceted pathogenesis of human disease. These limitations underscore the need for future investigations incorporating: 1) expanded clinical cohorts with precise molecular subtyping, 2) standardized disease classification protocols, and 3) development of next-generation animal models that better capture the immunopathological diversity of human PM.

In summary, we functionally link TIGIT deficiency to enhanced autoreactive CD4⁺ T-cell responses in patients with autoimmune myositis. Mechanistically, we provide the first demonstration in CD4⁺ T cells that cell-intrinsic TIGIT directly controls the differentiation of Th1 and Th17 cells through metabolic-epigenetic reprogramming (Supplementary Fig. 23). The data presented in this study could have significant implications for the treatment of T-cell-mediated autoimmune diseases.

Methods

Patients

Patients who fulfilled the 2017 EULAR/ACR Classification Criteria for adult PM⁶⁸ were recruited from the Department of Rheumatology and Clinical Immunology, the First Affiliated Hospital of Sun Yat-sen University. All of the recruited patients had active diseases based on MYOACT and elevated CK in the serum. Patients with DM⁶⁸ or SLE⁶⁹ were recruited as disease controls. Patients who were diagnosed with malignancy, infections, or other autoimmune diseases were excluded from this study. Age- and sex-matched HC were recruited as controls. Demographics of the patients and HC are summarized in Supplementary Table 1 and Supplementary Table 2. Informed consent and written consent forms were obtained before inclusion from all patients and HC, with approval from the Institutional Ethical Committee of the First Affiliated Hospital, Sun Yat-sen University ([2021]824 and [2021]816).



Mice

Tig1^{-/-} mice of C57BL/6 background were kindly provided by Professor Xingxu Huang from ShanghaiTech University as described previously⁷⁰. NOD-*Prkd*^{em26Cd52}*Il2rg*^{em26Cd22}/Gpt (NCG, Strain#T001475) and *Rag1*^{-/-} mice of C57BL/6 background (Strain#T004753) were purchased from GemPharmatech (Nanjing, China). Female 8–10-week-old

mice were used at the time of the experiment and were randomly assigned to experimental groups. Co-house *Tig1*^{+/+} mice served as controls. All experimental mice were housed under specific pathogen-free conditions and group-housed in a temperature-controlled environment (23 °C) on a 12 hours (h) light/dark cycle with *ad libitum* access to standard rodent chow at the Experimental Animal Center of Sun Yat-

Fig. 7 | TIGIT controls Th1 and Th17 cell differentiation through acetyl-CoA generation and histone acetylation. **a** ATP-citrate lyase (ACLY) controls the conversion of TCA-derived citrate into acetyl-coenzyme A (CoA) for histone acetylation. **b–f** CD4⁺ T cells from HC or PM patients were stimulated with α CD3/CD28 in the presence of UK5099 (20 μ M), recombinant human CD155-Fc (10 μ g/ml), or control IgG1 for 3 d. **b** Immunoblot analysis of ACLY expression in CD4⁺ T cells and representative bands of six biologically independent replicates. **c** Acetyl-CoA levels in whole-cell lysates and the cytosolic and mitochondrial fractions of CD4⁺ T cells and data from four biologically independent replicates. **d** Immunoblot analysis of H3K9 and H3K27 acetylation in CD4⁺ T cells from PM patients or HC. Representative bands of six biologically independent replicates. **e, f** Immunoblot analysis of ACLY and H3K9 and H3K27 acetylation in CD4⁺ T cells. Representative bands of four biologically independent replicates. **g–i** CD4⁺ T cells from *Tigit*^{+/+} or *Tigit*^{-/-} mice were stimulated with α CD3/CD28. **g** Immunoblot analysis of ACLY expression in mouse CD4⁺ T cells. **h** Acetyl-CoA in whole-cell lysates, cytosolic and mitochondrial fractions of mouse CD4⁺ T cells. Data from four biologically independent replicates. **i** Immunoblot analysis of acetylated H3K9 and H3K27 in mouse CD4⁺ T cells and

representative bands. **j, k** CD4⁺ T cells from HC or PM were stimulated with α CD3/CD28 in the presence of UK5099, ETO or BPTES for 3 d. Immunoblot analysis of ACLY (**j**), acetylated H3K9 and H3K27 (**k**) in CD4⁺ T cells. **l, m** *Tigit*^{-/-} or *Tigit*^{+/+} CD4⁺ T cells were stimulated with α CD3/CD28 in the presence of UK5099, ETO, or BPTES for 3 d. Immunoblot analysis of ACLY (**l**), acetylated H3K9 and H3K27 (**m**) in mouse CD4⁺ T cells treated with UK5099, ETO, or BPTES. **n** Quantification of H3K9 and H3K27 acetylation in CD4⁺ T cells from *Tigit*^{-/-} or *Tigit*^{+/+} mice at the *Il17a*, *Il17f*, and *Irfng* promoters and CNS2 and CNS22 by ChIP-qPCR. **o–t** Naive CD4⁺ T cells were cultured under Th1 or Th17 conditions in the presence of C646 (1 μ M) or vehicle for 5 d. Flow cytometric analysis of the expression of T-bet, IFN γ (**o–q**), ROR γ t, and IL-17A (**r–t**) in CD4⁺ T cells. For **c, h, p, q**, $n =$ four biologically independent replicates. **n** $n =$ three biologically independent replicates. **s, t**, $n =$ five biologically independent replicates. **e, f, j–m** The experiment was repeated three times independently with similar results. Data are mean \pm SEM. Statistics were performed using one-way ANOVA followed by multiple comparisons adjustments for **c** and **h**, two-tailed unpaired Student's t test for (**n**), and two-way ANOVA followed by multiple comparisons adjustments for **p, q, s, t**.

sen University. The ambient humidity was maintained at 40–60%. The study protocol for the mouse experiments was approved by the Ethics Committee of Sun Yat-sen University (2022000554, 2024003409), and all experiments were performed in accordance with the National Institutes of Health Guide for Care and Use of Animals.

Cell isolation

For human CD4⁺ T-cell purification, blood samples were collected from patients with PM or HC. The samples were processed within 2 h after collection, and PBMCs were freshly isolated by density gradient centrifugation. Human total and naive CD4⁺ T-cell enrichment was achieved by negative selection using EasySep™ Isolation Kit (STEMCELL Technologies, Catalog (Cat# 17952 and 17555)). For mouse CD4⁺ T-cell purification, a single-cell suspension of mouse splenocytes was prepared as we described previously⁷¹. Briefly, mouse spleens were cut into pieces and smashed with a syringe plunger. The cells were then filtered through a 70 μ m cell strainer (BD Bioscience, Cat# BD352350). Mouse total and naive CD4⁺ T cells were isolated by negative selection using magnetic beads (STEMCELL Technologies, Cat# 19852 and 19765). The purity of the cell population was over 95% as confirmed by flow cytometry (LSR Fortessa, BD Bioscience).

T-cell cultures

For in vitro cell culture, mouse CD4⁺ T cells were cultured in complete medium: advanced RPMI 1640 medium (Thermo Fisher Scientific, Cat# 12633012) supplemented with 10% FBS (Procell, Cat# 164210), 2 mM L-glutamine (MCE, Cat# HY-N0390), 55 μ M 2-mercaptoethanol (β -ME, Gibco, Cat# 21985023), and 1% penicillin/streptomycin (Gibco, Cat# 15140122). Human CD4⁺ T cells were cultured in complete medium without β -ME. Human and mouse CD4⁺ T cells were cultured at 37 °C in an incubator with 5% CO₂.

T-cell activation and differentiation

For T-cell activation assessment, human and mouse total CD4⁺ T cells were activated with anti-CD3/CD28 beads (Thermo Fisher Scientific, Cat# 11132D, 11453D) at a ratio of 1:2 for the indicated time. The differentiation of human and mouse Th cells was induced as previously described^{17,72,73}. Human naive CD4⁺ T cells were stimulated with anti-CD3/CD28 beads and cultured under different Th cell-polarizing conditions: Th1 cells: anti-IL-4 antibody (Clone# MP4-25D2, 10 μ g/ml, BioLegend, Cat# 500838), IL-12 (10 ng/ml, Sino Biological, Cat# CT011-H08H), and IL-2 (20 ng/ml, PeproTech, Cat# 200-02-10). Th2 cells: anti-IFN γ antibody (Clone# B27, 10 μ g/ml, BioLegend, Cat# 506532), IL-4 (10 ng/ml, PeproTech, Cat# 200-02-20) and IL-2 (20 ng/ml, PeproTech, Cat# 200-02-10); Th17 cells: TGF β 1 (2 ng/ml, PeproTech, Cat# 100-21-2), IL-6 (40 ng/ml, PeproTech, Cat# 200-06-5), and IL-23 (30 ng/ml, PeproTech, Cat# 200-23-2). Treg cells: TGF β 1 (5 ng/ml) and IL-2 (10 ng/ml).

Mouse naive CD4⁺ T cells were stimulated with anti-CD3/CD28 beads and polarized under different conditions: Th1 cells: anti-IL-4 antibody (Clone# 11B11, 5 μ g/ml, BioLegend, Cat# 504102), IL-12 (20 ng/ml, PeproTech, Cat# 210-12-2), and IL-2 (20 ng/ml, Sino Biological, Cat# 51061-MNAE). Th2 cells: anti-IFN γ antibody (Clone# R4-6A2, 5 μ g/ml, BioLegend, Cat# 505702), IL-4 (20 ng/ml, Sino Biological, Cat# 51084-MNAE), and IL-2 (20 ng/ml). Th17 cells: anti-IFN γ antibody (5 μ g/ml), anti-IL-4 antibody (5 μ g/ml), TGF β 1 (2 ng/ml, Sino Biological, Cat# 80116-RNAH-5), IL-6 (40 ng/ml, Sino Biological, Cat# 50136-MNAE), IL-23 (30 ng/ml, NovoProtein, Cat# C03U), and IL-1 β (20 ng/ml, Sino Biological, Cat# 50101-MNAE). Treg cells: anti-IFN γ antibody (5 μ g/ml), anti-IL-4 antibody (5 μ g/ml), TGF β 1 (5 ng/ml), and IL-2 (10 ng/ml). In some experiments, UK5099 (Cat# HY-15475), MSDC-0206 (Cat# HY-108022), ETO (Cat# HY-50202), BPTES (Cat# HY-12683), PI-103 (Cat# HY-10115, all from MCE), C646 (Cat# S7152), or BEZ235 (Cat# S1009, both from Selleck) were added to the cell culture at the indicated concentrations and time points. Alternatively, TIGIT was stimulated with recombinant human CD155-Fc chimera protein (Sino Biological, cat# 10109-H02H) plate-bound at 10 μ g/ml. As an isotype control, we used IgG1 (Sigma, Cat# I5154).

T-cell proliferation

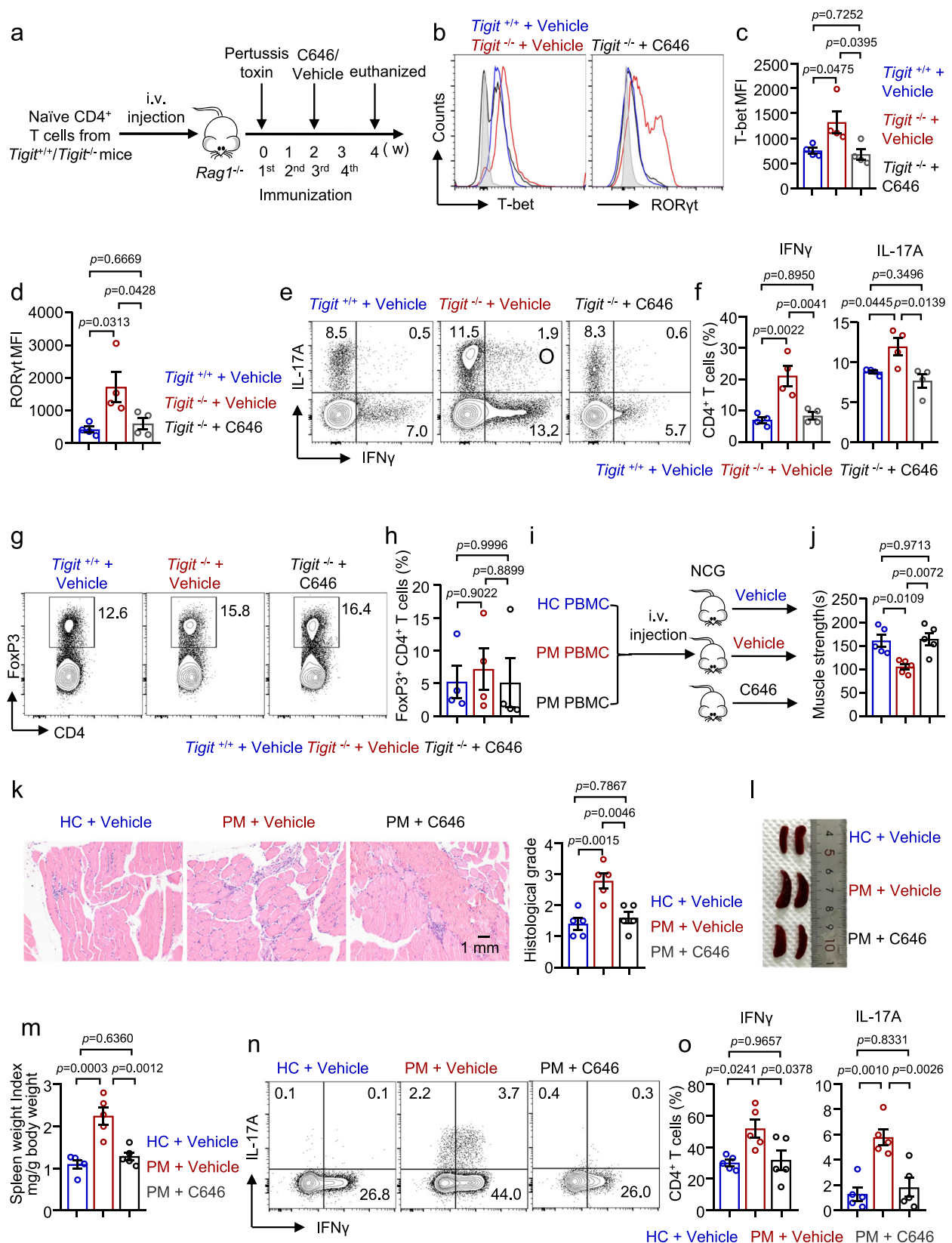
To analyze T-cell proliferation, purified human or mouse total CD4⁺ T cells (1×10^5) were labeled with 5 μ M carboxyfluorescein succinimidyl amino ester (CFSE, Thermo Fisher Scientific, Cat# C34554) and stimulated with anti-CD3/CD28 beads for 3 d. T-cell proliferation rates were assessed by flow cytometry.

Transfection of T cells

Electroporation was performed on human T cells using the P3 Primary Cell 4D-Nucleofector X Kit L (Lonza, Cat# V4XP-3024) according to the manufacturer's instructions. For TIGIT overexpression, total CD4⁺ T cells were transfected with 5 μ g of plasmid DNA using program EO-115. For TIGIT knockdown, naive CD4⁺ T cells were stimulated with anti-CD3/CD28 beads for 1 d before transfection with *TIGIT* siRNA (120 nM, Sangon, Cat# H540013-0001) under the same conditions. After the transfection, T cells were allowed to rest for 5 h to recover from electroporation. The overexpression and knockdown efficiency were validated by Western blot and flow cytometry.

Flow cytometry

For cell surface staining, cells were stained with the following antibodies: human CD3, CD4, CD8, TIGIT, CD226, CD96, CD44, CD25, HLA-DR, CD28 or mouse CD3, CD4, CD8, TIGIT, CD226, CD96, CD44, CD62L, CD69, CD25, and CD28 in the dark at 4 °C for 30 min. For intracellular cytokine staining, cells were treated with a cocktail



containing 50 ng/ml PMA (Cat# P8139), 500 ng/ml ionomycin (Cat# I0634), and 5 μ M brefeldin A (Cat# B7651, all from Sigma) at 37 °C for 4.5 h. After surface staining, cells were fixed and permeabilized with Fixation/Permeabilization solution (BD Biosciences, Cat# 554722), followed by incubation with the following antibodies: anti-human PE-IFN γ , anti-human Brilliant Violet 605-IL-17A, anti-human APC/CY7-TNF,

anti-human Brilliant Violet 421-IL-4, or anti-mouse APC/CY7-IFN γ , anti-mouse APC-IL-17A, anti-mouse FITC-TNF, anti-mouse PE-IL-4, anti-mouse APC-IL-2 in the dark at 4 °C for 30 min. For detection of transcriptional factors, cells were fixed and permeabilized using a FoxP3 Staining Set (eBioscience, Cat# 554714), followed by incubation with the following antibodies: anti-human/mouse PE/CY7-Tbet, anti-

Fig. 8 | TIGIT controls muscle inflammation by regulating Th1 and Th17 cell differentiation epigenetically in EAM. **a** Naive CD4⁺ T cells from *Tigit*^{+/+} or *Tigit*^{-/-} mice were adoptively transferred into *Rag1*^{-/-} mice. EAM was induced as shown in Fig. 2 and treated with C646 (10 mg/kg/d) or vehicle. **b–f** T-bet, RORγt, IFNγ, and IL-17A expression in CD4⁺ T cells from the spleens of *Tigit*^{+/+} or *Tigit*^{-/-} mice was measured by flow cytometry. **g, h** FoxP3 expression in CD4⁺ T cells was measured by flow cytometry. **i** NCG mice were immune reconstituted with PBMCs from five independent HC or PM patients. Four weeks later, the mice were treated with C646 (10 mg/kg/d) for 2 weeks. **j** Muscle strength of mice that received HC or PM PBMCs treated with vehicle or C646. **k** HE staining and histological score of muscle

(quadriceps) sections from mice that received HC or PM PBMCs treated with vehicle or C646. Original magnification: ×100. **l, m** Image showing spleen size in mice that received HC or PM PBMCs treated with vehicle or C646. Spleen weight index was calculated by dividing spleen weight (mg) by body weight (g). **n, o** IFNγ and IL-17A expression in CD4⁺ T cells from the spleen was measured by flow cytometry. **c, d, f, h** *n* = four biologically independent replicates. **j, k, m, n** *n* = five biologically independent replicates from five individual mice per group. All data are mean ± SEM. Statistics were done by one-way ANOVA followed by adjustments for multiple comparisons.

mouse/rat/human Alexa Fluor 488-FoxP3, anti-human/mouse Alexa Fluor 488-GATA3, anti-mouse PE-RORγt, anti-human PE/CY7-RORγt.

To measure the phosphorylation of AKT and S6, cells were fixed and permeabilized using the Fixation/Permeabilization solution (BD Biosciences, Cat# 554722). The cells were then stained with antibodies against p-AKT (Ser473) or p-S6 (Ser235/236), followed by goat anti-rabbit IgG secondary antibody.

To assess cell viability, cells were stained with the Annexin V-APC/7-AAD Apoptosis Kit (MultiSciences, Cat# 70-AP101) or Zombie Red (Biolegend, Cat# 423110) by flow cytometry. Details of all the FACS antibodies are shown in Supplementary Table 3. All the FACS samples were analyzed by a flow cytometer (LSR Fortessa, BD Bioscience).

Mitochondrial staining

The mitochondrial mass and mitochondrial potential of T cells were measured using MitoTracker Green (MTG, 50 nM, Invitrogen, Cat# M7514) and MitoTracker Deep Red (100 nM, Thermo Fisher Scientific, Cat# M22426), respectively, according to the manufacturers' instructions. Cells were analyzed by flow cytometry.

Western blot

T cells were lysed in RIPA lysis buffer, and protein concentrations were determined via a BCA assay (EpiZyme, Cat# ZJ101). SDS-PAGE-separated proteins were transferred to a polyvinylidene difluoride membrane (Millipore) via the wet transfer method. Membranes were incubated with antibodies against H3K9ac, H3K27ac, p-PI3K (p85 (Tyr458)/p55 (Tyr199), p-AKT (Ser473), p-S6 (S235/236), p-mTOR (Ser2448), mTOR, Raptor, TIGIT, IKKα, IKKβ, p-IkBα (Ser32), IκBα, p-p65 (Ser536), p65, ZAP70, p-ZAP70, LCK, p-LCK, β-actin, ACSS1, ACSS2, ACLY, p-CD226, and histone H3 at 4 °C overnight. The primary antibodies used were identified with horseradish peroxidase-labeled anti-rabbit or anti-mouse secondary antibodies. Signals were visualized with a Chemiluminescent™ Plus Western Blot Enhancing Kit (Millipore). Details of all the antibodies used in the western blot are shown in Supplementary Table 4. Source data are provided as a [Source Data](#) file.

Calcium flux

To detect intracellular calcium flux, purified *Tigit*^{+/+} or *Tigit*^{-/-} naive CD4⁺ T cells (2 × 10⁶ cells/ml) were labeled with Fluo-3 AM (5 μM, Solarbio, Cat# F8840) at 37 °C for 30 min and monitored by flow cytometry (LSR Fortessa, BD Bioscience). Following washing with Ca²⁺-free buffer, cells were incubated at room temperature (RT) to allow sufficient cleavage of AM esters, thereby rendering the probe impermeable to the cells. The cells were subsequently incubated with an anti-CD3-biotin antibody (10 μg/ml, Biolegend, Cat# 100303) at RT for 20 min, washed, and resuspended in 1 × PBS. Streptavidin (1 μg/ml, Sigma, Cat# S4762) was added to induce crosslinking and TCR signaling during the monitoring of calcium influx by flow cytometry. To quantify Ca²⁺ flux in CD4⁺ T cells, FlowJo software (BD Biosciences) was used to calculate the area under the curve (AUC) of each calcium flux plot. Each plot was divided into 19 regions, with the first four representing the pre-crosslinker baseline. The mean AUC of these regions was subtracted from the remaining regions to account for background fluorescence. Region 5, corresponding to the tube removal gap, was excluded.

Glucose uptake

Glucose uptake was evaluated and analyzed by the fluorescent glucose analog 2-NBDG (Thermo Fisher Scientific, Cat# N13195). Briefly, CD4⁺ T cells were cultured in glucose-free RPMI 1640 medium containing 20 μM 2-NBDG at 37 °C for 30 min. The amount of 2-NBDG uptake was analyzed by flow cytometry.

Lipid uptake and lipid content

To assess lipid uptake by T cells, T cells were incubated with medium (1% FBS) containing the fluorescent fatty acid analog Bodipy_{500/510} (1 μM, Thermo Fisher Scientific, Cat# D3793) at 37 °C for 30 min. To measure lipid content in T cells, cells were stained with Bodipy_{493/503} (2 μM, Thermo Fisher Scientific, Cat# D3922) probes at RT for 25 min. Cells were then collected and analyzed by flow cytometry.

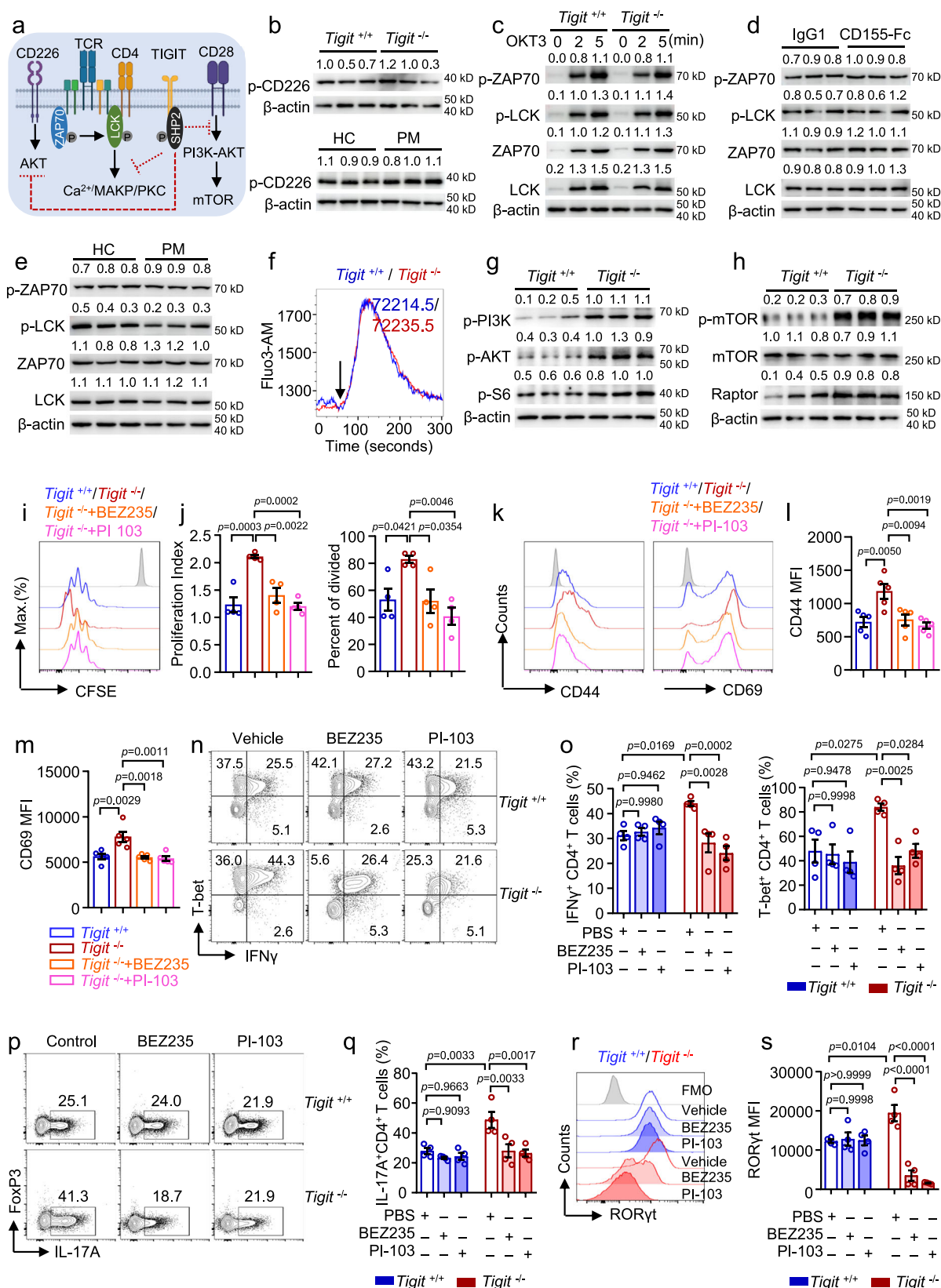
Seahorse assay

OCR and ECAR were assessed using the Cell Mito Stress Test Kit and Glycolysis Stress Test Kit, as previously described (Agilent, Cat# 103015-100, 103020-100)^{71,72}. CD4⁺ T cells were plated at 2 × 10⁵ cells per well in a Seahorse XF96 plate (Agilent) and attached using Cell-Tak (Corning, Cat# 354240). To measure mitochondrial respiration, CD4⁺ T cells were sequentially treated with oligomycin (1.5 μM), carbonyl cyanide-p-trifluoromethoxyphenylhydrazide (1.5 μM), and rotenone/antimycin A (R/A, 1.0 μM). To measure glycolytic activity, the cells were subsequently treated with glucose (10 mM), oligomycin (1 μM), and 2-DG (50 mM). Results were collected with Wave software version 2.6.1 (Agilent Technologies).

Stable isotope labeling and metabolomics

Stable isotope labeling (SIL) experiments were performed with in vitro-activated T cells via GC/MS or LC/MS⁷⁴. Briefly, CD4⁺ T cells were activated with anti-CD3/CD28 beads in RPMI containing 2 g/L ¹²C-glucose for 3 d. T cells were then collected and labeled in modified RPMI 1640 containing 2 g/L [¹³C₆]-glucose (MCE, Cat# HY-B0389A) for 24 h. For GC-MS, cells were plated at 2 × 10⁶ cells/well in 24-well plates. For LC-MS, cells were plated at 1 × 10⁷ cells/well in six-well plates.

For metabolic profiling of mouse CD4⁺ T cells, GC/MS was performed as previously described⁷⁴. In brief, metabolites were extracted using 500 μl of ice-cold HPLC-grade 80% methanol and vortexed briefly, followed by the addition of 200 μl of HPLC-grade water and then 500 μl of HPLC-grade chloroform. The mixture was vortexed and centrifuged to achieve phase separation. The supernatants were dried by vacuum spin for subsequent derivatization. The remaining mixture was then incubated with 2% (wt/vol) methoxyamine hydrochloride in pyridine at 37 °C for 60 min and silylated with N-methyl-N-(tert-butyldimethylsilyl) trifluoroacetamide with 1% tert-butyldimethylchlorosilane at 45 °C for 30 min. The [¹³C₆]-glucose derivatives were analyzed using a Thermo 1310 system coupled with an ISQ QD mass spectrometer. Data processing was performed using Trace Finder 3.2 software and MATLAB-based INCA software. The target compounds were qualitatively analyzed by selecting characteristic *m/z* ions and quantitatively analyzed using valine as internal standards for polar metabolites.



For metabolic profiling of human CD4⁺ T cells, LC/MS was performed as previously described⁷⁴. In brief, 400 µl of ice-cold HPLC-grade 80% methanol was added to each tube containing the cell samples, and the cells were sonicated. The tubes were then centrifuged at 18,000 × *g* at 4 °C for 15 min. The supernatant was collected and concentrated by centrifugation. The residues were redissolved in

100 µl of ice-cold HPLC-grade 80% methanol and then analyzed by ultrahigh-pressure LC-triple quadrupole mass spectrometer (UPLC-TQMS). The raw data from UPLC-TQMS were analyzed using Waters' MassLynx software (v4.1, Waters) for peak extraction, integration, identification, and quantification of the metabolites. R language (v4.1.1) was used for subsequent statistical analysis.

Fig. 9 | TIGIT dampens CD28 signaling in CD4⁺ T cells. **a** Scheme of TIGIT signaling in CD4⁺ T cells. Red dashed lines: potential downstream targets of TIGIT (Figure partially created in BioRender. Zhang, H. (2025) <https://BioRender.com/k1231h>). **b** Immunoblot analysis of p-CD226^{S329} in CD4⁺ T cells from *Tigit*^{-/-} or *Tigit*^{+/+} mice (upper) or CD4⁺ T cells from HC and PM patients (lower). Bands representative of three independent experiments with similar results are shown. **c** CD4⁺ T cells from *Tigit*^{-/-} or *Tigit*^{+/+} mice were stimulated with OKT3 for the indicated times. Immunoblot analyses of p-ZAP70^{Y319}, p-LCK^{Y505}, ZAP70, and LCK in CD4⁺ T cells and representative bands of three independent experiments with similar results. **d** Immunoblot analysis of p-ZAP70^{Y319}, p-LCK^{Y505}, ZAP70, and LCK in HC CD4⁺ T cells treated with recombinant CD155-Fc or the IgG1 control. Representative bands of three independent experiments with similar results. **e** Immunoblot analysis of the expression of p-ZAP70^{Y319}, p-LCK^{Y505}, ZAP70, and LCK in CD4⁺ T cells from HC and PM patients. Representative bands of three independent experiments with similar results. **f** Calcium influx into *Tigit*^{-/-} or *Tigit*^{+/+} CD4⁺ T cells was recorded by flow cytometry as stimulated with anti-CD3-biotin antibody (10 µg/ml) followed by crosslinking (arrow) with Streptavidin. The area under the curve (AUC) was

measured by flow cytometry. **g, h** *Tigit*^{-/-} or *Tigit*^{+/+} CD4⁺ T cells were activated with αCD3/CD28 for 3 d. Immunoblot analysis of p-PI3K^{P85}, p-AKT^{S473}, and p-S6^{S235/236} (**g**) and p-mTOR, mTOR, and Raptor (**h**). Representative bands of three independent experiments with similar results. **i, j** CD4⁺ T cells from *Tigit*^{-/-} or *Tigit*^{+/+} mice were labeled with CFSE and stimulated with anti-CD28 plus PMA in the presence of BEZ235 (1 µM), PI-103 (0.5 µM), or vehicle for 3 d. The frequency of proliferated cells was calculated via flow cytometry and data from four biologically independent replicates. **k–m** *Tigit*^{-/-} or *Tigit*^{+/+} CD4⁺ T cells were stimulated with anti-CD28 plus PMA in the presence of BEZ235 (1 µM), PI-103 (0.5 µM), or vehicle for 48 h. CD44 and CD69 expression in CD4⁺ T cells were measured by flow cytometry, and data from five biologically independent replicates. **n–s** Naive CD4⁺ T cells from *Tigit*^{-/-} or *Tigit*^{+/+} mice were polarized under Th1 or Th17 conditions for 5 d. IFN γ , T-bet, ROR γ t, and IL-17A expression in CD4⁺ T cells was measured via flow cytometry. Data from five biologically independent replicates. All data are expressed as mean \pm SEM. Statistics were done by one-way ANOVA in **j, l, m**, or two-way ANOVA in **o, q, s**. Multiple comparisons were performed for adjustment.

Detection of subcellular acetyl-CoA

Acetyl-CoA concentrations in the subcellular fractions were determined via an acetyl-CoA assay kit (Solarbio, Cat# BC0980). Briefly, 5×10^6 CD4⁺ T cells were harvested in 200 µl of extraction buffer containing 0.25 M sucrose, 20 mM HEPES, 10 mM KCl, 2 mM MgCl₂, 1 mM EDTA, 1 mM EGTA, and 1 mM dithiothreitol. Samples were incubated on ice for 30 min, followed by homogenization with a Teflon-glass homogenizer with 20–30 up-and-down passes of the pestle. Nuclei and unbroken cells were removed as pellets after centrifugation at $800 \times g$ for 10 min at 4 °C. The resulting supernatants were further centrifuged at $10,000 \times g$ for 15 min at 4 °C to collect the cytosolic fractions. The pellet obtained from this step was washed once with ice-cold PBS and then sonicated for 3 s at 200 watts 30 times, followed by centrifugation at $13,000 \times g$ for 5 min at 4 °C to collect the mitochondrial fractions. For the quantification of total cellular acetyl-CoA levels, cells were sonicated and centrifuged at $8000 \times g$ at 4 °C for 10 min. Acetyl-CoA levels were quantified according to the manufacturer's instructions. The absorbance was recorded with a spectrophotometer (Shimadzu) at 340 nm.

Plasmid construction

To rescue TIGIT expression in CD4⁺ T cells from PM patients, a TIGIT overexpression plasmid was constructed by cloning the human *TIGIT* (*hTIGIT*) gene into the pcDNA3.1 (+) plasmid. The mRNA isolated from human PBMCs was reverse transcribed into complementary DNA (cDNA) via reverse transcriptase. *TIGIT* was then amplified with the following primers: forward primer (5'-cttggtaccgagctcgatccGCCAC-CATGCGCTGGTGtctctcc-3') and reverse primer (5'-tgctggatctcgagaattcCTAACCAGTCTCTGTGAAGAAGCTGC-3'), using 2 \times Phanta Flash Master Mix (Vazyme Biotech, Cat# P510-01). After digestion with the restriction endonucleases BamHI (Cat# JB101-01) and EcoRI (Cat# JE201-01) (Both from TransGen Biotech), the pcDNA3.1-*hTIGIT* overexpression plasmid was constructed via a MultiS One Step Cloning Kit (Vazyme Biotech, Cat# C113-01) according to the manufacturer's instructions. Genetic components were confirmed by sequencing (BGI).

Real-time PCR

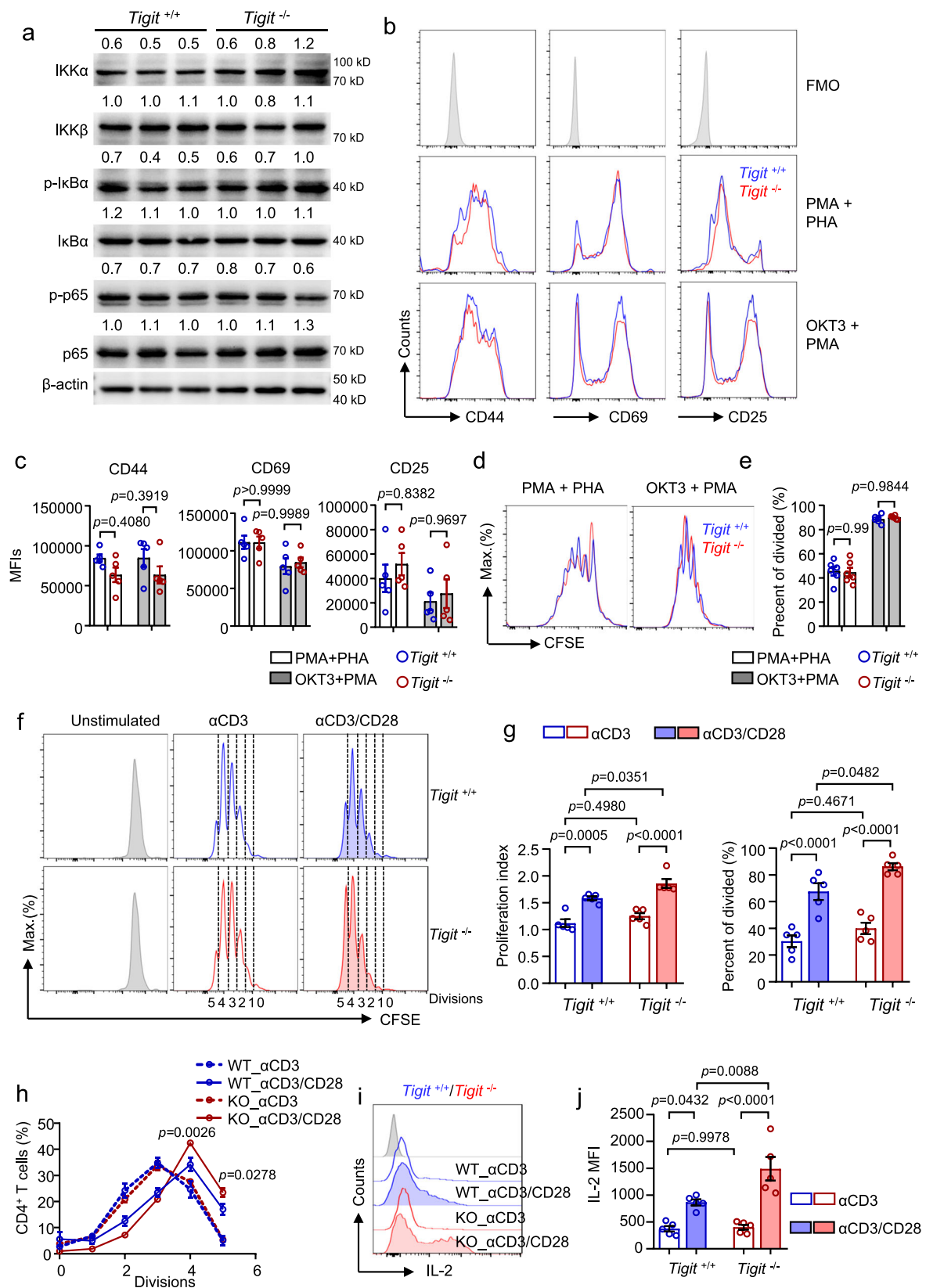
Real-time PCR (qPCR) was performed to measure mRNA expression. Briefly, total mRNA was extracted via TRIzol (Invitrogen, Cat# 15596018). Complementary DNA was synthesized with a reverse transcription kit (Accurate Biotechnology, Cat# AG11706). The protocol for SYBR Green (Accurate Biotechnology, Cat# AG11718)-based qPCR was set at an initial denaturation of 30 s at 95 °C, followed by 40 cycles of 5 s denaturation at 95 °C and 30 s annealing/extension at 60 °C. All the target genes were relative to β -actin. All sequences of the primers used in the study are listed in Supplementary Table 5.

ChIP-qPCR

For ChIP followed by qPCR, CD4⁺ T cells were stimulated with anti-CD3/CD28 beads for 3 d and restimulated with PMA (50 ng/ml) and ionomycin (500 ng/ml) for 3 h. The cells were fixed with 1% formaldehyde (Macklin, Cat# F809702) at 37 °C for 10 min. The reaction was then quenched by incubation with glycine (125 mM) at RT for 5 min. The cells were washed with cold PBS containing 1 mM PMSF three times, and the nuclei were isolated in SDS lysis buffer from a ChIP Assay Kit (Beyotime Biotechnology, Cat# P2078). After 10 min of incubation on ice, the nuclear lysates were sonicated via a Biorupter Plus Sonication system (Diagenode) for 30 cycles at high power (20 s on, 20 s off). Histone–DNA complexes were isolated using polyclonal anti-mouse antibodies against acetylated histone H3 lysine 9 (H3K9ac) and acetylated histone H3 lysine 27 (H3K27ac). Briefly, protein A + G agarose/salmon sperm DNA was used to preclear the whole-cell lysate at 4 °C for 30 min. After the 2% input sample was extracted, the samples were divided equally and incubated with anti-H3K9ac (1:50, Cell Signaling Technology, Cat# 9649) and anti-H3K27ac antibodies (1:100, Cell Signaling Technology, Cat# 8173) or control IgG (Millipore, Cat# 12-370) at 4 °C overnight with slow rotation. Protein A + G agarose/salmon sperm DNA was then added and incubated at 4 °C for 1 h. The beads were sequentially washed with low-salt immune complex washing buffer, high-salt immune complex washing buffer, LiCl immune complex washing buffer, and TE buffer (twice) at 4 °C with rotation for 5 min each. The DNA–protein complexes were eluted with elution buffer (1% SDS and 0.1 M NaHCO₃) and decrosslinked by adding 0.2 M NaCl and heating at 65 °C for 4 h. The proteins were then digested with proteinase K at 45 °C for 1 h. The DNA segments were purified with a DNA Purification Kit (Beyotime Biotechnology, Cat# D0033) and used for qPCR. The primers used for ChIP-qPCR are listed in Supplementary Table 6. The results were normalized to both the input and the isotype control.

Bulk RNA-seq

CD4⁺ T cells from *Tigit*^{-/-} or *Tigit*^{+/+} mice were stimulated with anti-CD3/CD28 beads for 3 d. RNA libraries were sequenced on a BGISEQ500 platform (BGI) to generate paired-end 150-base reads. The reads were aligned against the human reference genome (GRCh38) via HISAT2 (version 2.2.1). By using featureCounts (version 2.0.1), the read counts of genes were further quantified. Genes with more than 10 reads in total across all samples were adopted for further analysis. The Sva package was used for the removal of batch effects by applying the ComBat-seq function⁷⁵. DEGs under different conditions were analyzed using DESeq2 (version 1.28.1) R package⁷⁶ via a moderated t test of Benjamini–Hochberg (BH) method. The cutoff values for significant DEGs were set as adjusted $p < 0.01$ and $|\log_2$ (fold change)| > 0.05 . ClusterProfiler⁷⁷ (version 4.1.0) R package was used to assign biological functions, including GO, KEGG, RPD, and WP signaling pathways, to the



DEGs. GSEA⁷⁸ was also applied to evaluate signaling pathways enriched in different treatment groups. The normalized enrichment score (NES) was used for the estimation of enrichment. The enriched signaling pathway was set at the threshold of p value < 0.05 . The RNA-seq data were analyzed and visualized via R (version 4.0.5) and RStudio (integrated development for R; RStudio).

Adoptive transfer

Naive CD4⁺ T cells were isolated from the spleens of *Tigit*^{-/-} or *Tigit*^{+/+} mice as described above. *Rag1*^{-/-} mice were used as recipients and were injected with 2×10^6 naive mouse CD4⁺ T cells each intravenously.

Fig. 10 | TCR signaling is not involved with TIGIT-mediated T-cell suppression. **a** CD4⁺ T cells isolated from *Tigit*^{+/+} or *Tigit*^{-/-} mice were stimulated with α CD3/CD28 for 3 d. IKK α , IKK β , p-IkBa, IkBa, p-p65, and p65 expression were quantified by western blot. Data from six biologically independent replicates. **b, c** CD4⁺ T cells from *Tigit*^{+/+} or *Tigit*^{-/-} mice were stimulated with PMA + PHA or OKT3 + PMA for 48 h. CD44, CD69, and CD25 expression was measured by flow cytometry. Data from five biologically independent replicates. **d, e** CD4⁺ T cells isolated from *Tigit*^{+/+} or *Tigit*^{-/-} mice were labeled with CFSE and stimulated with PMA + PHA or OKT3 +

PMA for 3 d. T-cell proliferation was measured by flow cytometry. Data from six biologically independent replicates. **f–j** CD4⁺ T cells from *Tigit*^{+/+} or *Tigit*^{-/-} mice were stimulated with anti-CD3 alone (α CD3) or anti-CD3 plus anti-CD28 (α CD3/CD28) for 3 d. **f–h** CD4⁺ T cells were labeled with CFSE, and cell proliferation was assessed by flow cytometry. **i, j** IL-2 expression was assessed by flow cytometry. Representative histograms were shown. Data from five biologically independent replicates. All data are mean \pm SEM. Statistics were done by two-way ANOVA followed by adjustments for multiple comparisons.

Mouse experiments

The EAM model was established as described previously⁶⁷. Briefly, 8-week-old female *Tigit*^{-/-} or *Tigit*^{+/+} mice or *Rag1*^{-/-} mice reconstituted with *Tigit*^{-/-} or *Tigit*^{+/+} CD4⁺ T cells were injected with 500 ng pertussis toxin (MCE, Cat# HY-112779) intraperitoneally. The mice were subsequently immunized with 100 μ l of 50% complete Freund's adjuvant (Sigma, Cat# F5881) containing 1 mg of myosin (or with an equal volume of PBS in the control group) bilaterally on the sides of the hind foot pads, tail base, and flanks four times at 1-week intervals.

For TIGIT agonist studies, EAM mice were randomized into an anti-TIGIT agonistic antibody group or an isotype control group. The mice were treated with an anti-TIGIT antibody (10 mg/kg, BioXcell, Cat# BE0274) or a mouse IgG1 isotype control (BioXcell, Cat# BE0083) every 3 d via intraperitoneal injection after the second immunization for 2 weeks. To study the role of histone acetylation in EAM, EAM mice were randomized into the C646 or vehicle group. After the second immunization, the mice were treated with C646 (10 mg/kg) or an equal volume of vehicle daily by intraperitoneal injection for 2 weeks.

Muscle strengths were assessed via an inverted screen test as previously described^{10,79}. The inverted screen consisted of a 43 \times 43 cm² wire mesh, framed by a 4 cm deep wooden border. The mesh was made up of 1 mm diameter wires, with each square measuring 12 mm. To perform the test, the mouse was positioned in the center of the grid, which was then gradually inverted and held 30 cm above a cushioned surface. The time taken for the mouse to fall was recorded. After treatment, the quadriceps muscles were collected for HE staining, RNA-seq, and qPCR. The sizes of the spleens were evaluated, and the spleen weight index was calculated. Spleens were collected for single-cell preparation and analyzed by flow cytometry.

Humanized mouse model

A humanized mouse model of PBMC-NCG chimera was generated as previously described with modifications⁶². To establish a humanized mouse model of myositis, PBMCs were collected from patients with PM or HC. Eight-week-old female NCG mice were intravenously injected with human PBMCs (1×10^7 /mouse) from PM patients or HC through the tail vein. After 4 weeks, NCG mice were treated with C646 (10 mg/kg/d) or an equal volume of vehicle by intraperitoneal injection for 2 weeks.

Statistics

All the data are presented as the mean \pm SEM. Statistical analysis was performed via Prism 9.0. Comparisons were assessed by two-tailed unpaired Student's *t* test within two groups. To compare data between three or more groups, one-way, two-way ANOVA with or without repeated measurements was performed, followed by multiple comparisons post-test. *p* < 0.05 was considered statistically significant in this study. Statistical methods are indicated in the figure legends for each panel.

Reporting summary

Further information on research design is available in the Nature Portfolio Reporting Summary linked to this article.

Data availability

All data supporting the findings of this study are available in the article and its Source Data, or from the corresponding authors upon request. The raw sequencing (Bulk RNA-Seq) data generated in this study have

been deposited in Gene Expression Omnibus under accession codes GSE274668 (<https://www.ncbi.nlm.nih.gov/geo/query/acc.cgi>) and GSE275016 (<https://www.ncbi.nlm.nih.gov/geo/query/acc.cgi>). The mass spectrometry raw data have been deposited in the iProX repository under the series numbers PXD055328 (<https://www.iprox.cn/page/project.html?id=IPX0009539000>) and PXD055329 (<https://www.iprox.cn/page/project.html?id=IPX0009540000>). Source data are provided with this paper.

References

- Zhao, L., Wang, Q., Zhou, B., Zhang, L. & Zhu, H. The role of immune cells in the pathogenesis of idiopathic inflammatory myopathies. *Aging Dis.* **12**, 247–260 (2021).
- Malmstrom, V., Venalis, P. & Albrecht, I. T cells in myositis. *Arthritis Res Ther.* **14**, 230 (2012).
- Sun, L., Su, Y., Jiao, A., Wang, X. & Zhang, B. T cells in health and disease. *Signal Transduct. Target. Ther.* **8**, 235 (2023).
- Jung, S. M. & Kim, W. U. Targeted immunotherapy for autoimmune disease. *Immune Netw.* **22**, e9 (2022).
- Mease, P. J., Helliwell, P. S., Hjuler, K. F., Raymond, K. & McInnes, I. Brodalumab in psoriatic arthritis: results from the randomised phase III AMVISION-1 and AMVISION-2 trials. *Ann. Rheum. Dis.* **80**, 185–193 (2021).
- Wei, J. C. et al. Efficacy and safety of brodalumab, an anti-IL17RA monoclonal antibody, in patients with axial spondyloarthritis: 16-week results from a randomised, placebo-controlled, phase 3 trial. *Ann. Rheum. Dis.* **80**, 1014–1021 (2021).
- Tournadre, A. et al. Th1 and Th17 balance in inflammatory myopathies: interaction with dendritic cells and possible link with response to high-dose immunoglobulins. *Cytokine* **46**, 297–301 (2009).
- Page, G., Chevrel, G. & Miossec, P. Anatomic localization of immature and mature dendritic cell subsets in dermatomyositis and polymyositis: Interaction with chemokines and Th1 cytokine-producing cells. *Arthritis Rheum.* **50**, 199–208 (2004).
- Chevrel, G. et al. Interleukin-17 increases the effects of IL-1 beta on muscle cells: arguments for the role of T cells in the pathogenesis of myositis. *J. Neuroimmunol.* **137**, 125–133 (2003).
- Lai, Y. et al. Iron controls T helper cell pathogenicity by promoting glucose metabolism in autoimmune myopathy. *Clin. Transl. Med.* **12**, e999 (2022).
- Liu, S., Liao, S., Liang, L., Deng, J. & Zhou, Y. The relationship between CD4(+) T cell glycolysis and their functions. *Trends Endocrinol. Metab.* **34**, 345–360 (2023).
- Chapman, N. M. & Chi, H. Metabolic adaptation of lymphocytes in immunity and disease. *Immunity* **55**, 14–30 (2022).
- Geltink, R. I. K., Kyle, R. L. & Pearce, E. L. Unraveling the complex interplay between T cell metabolism and function. *Annu. Rev. Immunol.* **36**, 461–488 (2018).
- MacIver, N. J., Michalek, R. D. & Rathmell, J. C. Metabolic regulation of T lymphocytes. *Annu. Rev. Immunol.* **31**, 259–283 (2013).
- Puleston, D. J. et al. Polyamine metabolism is a central determinant of helper T cell lineage fidelity. *Cell* **184**, 4186–4202.e4120 (2021).
- Peng, M. et al. Aerobic glycolysis promotes T helper 1 cell differentiation through an epigenetic mechanism. *Science* **354**, 481–484 (2016).

17. Hochrein, S. M. et al. The glucose transporter GLUT3 controls T helper 17 cell responses through glycolytic-epigenetic reprogramming. *Cell Metab.* **34**, 516–532.e511 (2022).
18. Angiari, S. et al. Pharmacological activation of pyruvate kinase M2 inhibits CD4(+) T cell pathogenicity and suppresses Autoimmunity. *Cell Metab.* **31**, 391–405.e398 (2020).
19. Yin, Y. et al. Normalization of CD4+ T cell metabolism reverses lupus. *Sci. Transl. Med.* **7**, 274ra218 (2015).
20. Wang, S., Yang, N. & Zhang, H. Metabolic dysregulation of lymphocytes in autoimmune diseases. *Trends Endocrinol. Metab.* **35**, 624–637 (2024).
21. Manieri, N. A., Chiang, E. Y. & Grogan, J. L. TIGIT: a key inhibitor of the cancer immunity cycle. *Trends Immunol.* **38**, 20–28 (2017).
22. Yu, X. et al. The surface protein TIGIT suppresses T cell activation by promoting the generation of mature immunoregulatory dendritic cells. *Nat. Immunol.* **10**, 48–57 (2009).
23. Anderson, A. C., Joller, N. & Kuchroo, V. K. Lag-3, Tim-3, and TIGIT: co-inhibitory receptors with specialized functions in immune regulation. *Immunity* **44**, 989–1004 (2016).
24. Liu, S. et al. Recruitment of Grb2 and SHIP1 by the ITT-like motif of TIGIT suppresses granule polarization and cytotoxicity of NK cells. *Cell Death Differ.* **20**, 456–464 (2013).
25. Stanitsky, N. et al. The interaction of TIGIT with PVR and PVRL2 inhibits human NK cell cytotoxicity. *Proc. Natl. Acad. Sci. USA* **106**, 17858–17863 (2009).
26. Joller, N. et al. Cutting edge: TIGIT has T cell-intrinsic inhibitory functions. *J. Immunol.* **186**, 1338–1342 (2011).
27. Joller, N., Anderson, A. C. & Kuchroo, V. K. LAG-3, TIM-3, and TIGIT: distinct functions in immune regulation. *Immunity* **57**, 206–222 (2024).
28. Joller, N. et al. Treg cells expressing the coinhibitory molecule TIGIT selectively inhibit proinflammatory Th1 and Th17 cell responses. *Immunity* **40**, 569–581 (2014).
29. Banta, K. L. et al. Mechanistic convergence of the TIGIT and PD-1 inhibitory pathways necessitates co-blockade to optimize anti-tumor CD8(+) T cell responses. *Immunity* **55**, 512–526.e519 (2022).
30. Zhao, J. et al. TIGIT-Fc fusion protein alleviates murine lupus nephritis through the regulation of SPI-B-PAX5-XBP1 axis-mediated B-cell differentiation. *J. Autoimmun.* **139**, 103087 (2023).
31. Isenberg, D. A. et al. International consensus outcome measures for patients with idiopathic inflammatory myopathies. Development and initial validation of myositis activity and damage indices in patients with adult onset disease. *Rheumatology* **43**, 49–54 (2004).
32. Bird, J. J. et al. Helper T cell differentiation is controlled by the cell cycle. *Immunity* **9**, 229–237 (1998).
33. Wilfahrt, D. & Delgoffe, G. M. Metabolic waypoints during T cell differentiation. *Nat. Immunol.* **25**, 206–217 (2024).
34. Martinez-Reyes, I. & Chandel, N. S. Mitochondrial TCA cycle metabolites control physiology and disease. *Nat. Commun.* **11**, 102 (2020).
35. Sivanand, S., Viney, I. & Wellen, K. E. Spatiotemporal control of acetyl-CoA metabolism in chromatin regulation. *Trends Biochem. Sci.* **43**, 61–74 (2018).
36. Dufort, F. J. et al. Glucose-dependent de novo lipogenesis in B lymphocytes: a requirement for atp-citrate lyase in lipopolysaccharide-induced differentiation. *J. Biol. Chem.* **289**, 7011–7024 (2014).
37. Guertin, D. A. & Wellen, K. E. Acetyl-CoA metabolism in cancer. *Nat. Rev. Cancer* **23**, 156–172 (2023).
38. Lenschow, D. J., Walunas, T. L. & Bluestone, J. A. CD28/B7 system of T cell costimulation. *Annu. Rev. Immunol.* **14**, 233–258 (1996).
39. Shyer, J. A., Flavell, R. A. & Bailis, W. Metabolic signaling in T cells. *Cell Res.* **30**, 649–659 (2020).
40. Powell, J. D. & Delgoffe, G. M. The mammalian target of rapamycin: linking T cell differentiation, function, and metabolism. *Immunity* **33**, 301–311 (2010).
41. Faguet, G. B. Mechanisms of lymphocyte activation. Binding kinetics of phytohemagglutinin to human lymphocytes. *J. Biol. Chem.* **252**, 2095–2100 (1977).
42. Touraine, J. L. et al. Phorbol myristate acetate: a mitogen selective for a T-lymphocyte subpopulation. *J. Exp. Med.* **145**, 460–465 (1977).
43. Franco, C., Gatto, M., Iaccarino, L., Ghirardello, A. & Doria, A. Lymphocyte immunophenotyping in inflammatory myositis: a review. *Curr. Opin. Rheumatol.* **33**, 522–528 (2021).
44. McKinney, E. F., Lee, J. C., Jayne, D. R., Lyons, P. A. & Smith, K. G. T-cell exhaustion, co-stimulation and clinical outcome in autoimmunity and infection. *Nature* **523**, 612–616 (2015).
45. Yue, C. et al. TIGIT as a promising therapeutic target in autoimmune diseases. *Front. Immunol.* **13**, 911919 (2022).
46. Zhao, W. et al. TIGIT overexpression diminishes the function of CD4 T cells and ameliorates the severity of rheumatoid arthritis in mouse models. *Exp. Cell Res.* **340**, 132–138 (2016).
47. Mao, L. et al. TIGIT signalling pathway negatively regulates CD4(+) T-cell responses in systemic lupus erythematosus. *Immunology* **151**, 280–290 (2017).
48. Li, W. et al. Upregulation of the CD155-CD226 axis is associated with muscle inflammation and disease severity in idiopathic inflammatory myopathies. *Neurol. Neuroimmunol. Neuroinflamm.* **10**, e200143 (2023).
49. Chauvin, J. M. et al. TIGIT and PD-1 impair tumor antigen-specific CD8(+) T cells in melanoma patients. *J. Clin. Invest.* **125**, 2046–2058 (2015).
50. Johnston, R. J. et al. The immunoreceptor TIGIT regulates antitumor and antiviral CD8(+) T cell effector function. *Cancer Cell* **26**, 923–937 (2014).
51. Asashima, H. et al. Impaired TIGIT expression on B cells drives circulating follicular helper T cell expansion in multiple sclerosis. *J. Clin. Invest.* **132**, e156254 (2022).
52. Lozano, E., Dominguez-Villar, M., Kuchroo, V. & Hafler, D. A. The TIGIT/CD226 axis regulates human T cell function. *J. Immunol.* **188**, 3869–3875 (2012).
53. Peters, K. et al. TIGIT stimulation suppresses autoimmune uveitis by inhibiting Th17 cell infiltration. *J. Leukoc. Biol.* **116**, 1054–1060 (2024).
54. Soriano-Baguet, L. & Brenner, D. Metabolism and epigenetics at the heart of T cell function. *Trends Immunol.* **44**, 231–244 (2023).
55. Frauwirth, K. A. & Thompson, C. B. Regulation of T lymphocyte metabolism. *J. Immunol.* **172**, 4661–4665 (2004).
56. Frauwirth, K. A. et al. The CD28 signaling pathway regulates glucose metabolism. *Immunity* **16**, 769–777 (2002).
57. Patsoukis, N. et al. PD-1 alters T-cell metabolic reprogramming by inhibiting glycolysis and promoting lipolysis and fatty acid oxidation. *Nat. Commun.* **6**, 6692 (2015).
58. He, W. et al. CD155/TIGIT signaling regulates CD8(+) T-cell metabolism and promotes tumor progression in human gastric cancer. *Cancer Res.* **77**, 6375–6388 (2017).
59. Baixauli, F. et al. Mitochondrial respiration controls lysosomal function during inflammatory T cell responses. *Cell Metab.* **22**, 485–498 (2015).
60. Shin, B. et al. Mitochondrial oxidative phosphorylation regulates the fate decision between pathogenic Th17 and regulatory T cells. *Cell Rep.* **30**, 1898–1909.e1894 (2020).
61. Steinert, E. M., Vasan, K. & Chandel, N. S. Mitochondrial metabolism regulation of T cell-mediated immunity. *Annu. Rev. Immunol.* **39**, 395–416 (2021).
62. Wu, B. et al. Succinyl-CoA ligase deficiency in pro-inflammatory and tissue-invasive T cells. *Cell Metab.* **32**, 967–980.e965 (2020).
63. Mocholi, E. et al. Pyruvate metabolism controls chromatin remodeling during CD4(+) T cell activation. *Cell Rep.* **42**, 112583 (2023).
64. Li, M. et al. T-cell immunoglobulin and ITIM domain (TIGIT) receptor/poliovirus receptor (PVR) ligand engagement suppresses interferon-

- gamma production of natural killer cells via beta-arrestin 2-mediated negative signaling. *J. Biol. Chem.* **289**, 17647–17657 (2014).
65. Worboys, J. D. et al. TIGIT can inhibit T cell activation via ligation-induced nanoclusters, independent of CD226 co-stimulation. *Nat. Commun.* **14**, 5016 (2023).
 66. Zhang, H. et al. CD28 signaling controls metabolic fitness of pathogenic T cells in medium and large vessel vasculitis. *J. Am. Coll. Cardiol.* **73**, 1811–1823 (2019).
 67. Allenbach, Y. et al. Role of regulatory T cells in a new mouse model of experimental autoimmune myositis. *Am. J. Pathol.* **174**, 989–998 (2009).
 68. Lundberg, I. E. et al. 2017 European League Against Rheumatism/American College of Rheumatology Classification Criteria for adult and juvenile idiopathic inflammatory myopathies and their major subgroups. *Arthritis Rheumatol.* **69**, 2271–2282 (2017).
 69. Hochberg, M. C. Updating the American College of Rheumatology revised criteria for the classification of systemic lupus erythematosus. *Arthritis Rheum.* **40**, 1725 (1997).
 70. Chen, B. et al. TIGIT deficiency protects mice from DSS-induced colitis by regulating IL-17A-producing CD4(+) tissue-resident memory T cells. *Front. Immunol.* **13**, 931761 (2022).
 71. Zeng, Q. et al. Spleen fibroblastic reticular cell-derived acetylcholine promotes lipid metabolism to drive autoreactive B cell responses. *Cell Metab.* **35**, 837–854.e838 (2023).
 72. Li, M. et al. NAMPT is a metabolic checkpoint of IFN γ -producing CD4(+) T cells in lupus nephritis. *Mol. Ther.* **31**, 193–210 (2023).
 73. Yan, J., Pandey, S. P., Barnes, B. J., Turner, J. R. & Abraham, C. T cell-intrinsic IRF5 regulates T cell signaling, migration, and differentiation and promotes intestinal inflammation. *Cell Rep.* **31**, 107820 (2020).
 74. Roy, D. G. et al. Methionine metabolism shapes T helper cell responses through regulation of epigenetic reprogramming. *Cell Metab.* **31**, 250–266.e259 (2020).
 75. Leek, J. T., Johnson, W. E., Parker, H. S., Jaffe, A. E. & Storey, J. D. The sva package for removing batch effects and other unwanted variation in high-throughput experiments. *Bioinformatics* **28**, 882–883 (2012).
 76. Love, M. I., Anders, S., Kim, V. & Huber, W. RNA-Seq workflow: gene-level exploratory analysis and differential expression. *F1000Res.* **4**, 1070 (2015).
 77. Wu, T. et al. clusterProfiler 4.0: a universal enrichment tool for interpreting omics data. *Innovation* **2**, 100141 (2021).
 78. Subramanian, A. et al. Gene set enrichment analysis: a knowledge-based approach for interpreting genome-wide expression profiles. *Proc. Natl Acad. Sci. USA* **102**, 15545–15550 (2005).
 79. Contet, C., Rawlins, J. N. & Deacon, R. M. A comparison of 129S2/SvHsd and C57BL/6JOLA-Hsd mice on a test battery assessing sensorimotor, affective and cognitive behaviours: implications for the study of genetically modified mice. *Behav. Brain Res.* **124**, 33–46 (2001).

Acknowledgements

This work is supported by the National Natural Science Foundation of China (82402113, 82471764, 92474103, 82071819) and the Fundamental Research Funds for the Central Universities (22hytd11).

Author contributions

H.Z. conceived, designed, and supervised the project. Y.L., Shuang W., T.R., X.R., X.W., and M.L. performed the experiments. Y.Q. designed and constructed the plasmids. J.S. performed the transcriptome-wide data analyses. Y.L. performed the LC–MS/GC–MS analyses. Shuyi, W., Shuang W., M.Z., L.Z., and M.L. collected and processed the clinical samples. Y.H. and N.Y. analyzed the clinical data. Z.K. performed a pathological assessment of muscle tissue. Y.L., H.Z., and R.W. analyzed the statistics. H.Z. and Y.L. drafted the manuscript with feedback from all the authors.

Competing interests

The authors declare no competing interests.

Additional information

Supplementary information The online version contains supplementary material available at <https://doi.org/10.1038/s41467-025-59786-z>.

Correspondence and requests for materials should be addressed to Hui Zhang.

Peer review information *Nature Communications* thanks Robert J. Johnston, who co-reviewed with Ruozhen Hu, and Hu Zeng, and the other, anonymous, reviewer(s) for their contribution to the peer review of this work. A peer review file is available.

Reprints and permissions information is available at <http://www.nature.com/reprints>

Publisher's note Springer Nature remains neutral with regard to jurisdictional claims in published maps and institutional affiliations.

Open Access This article is licensed under a Creative Commons Attribution-NonCommercial-NoDerivatives 4.0 International License, which permits any non-commercial use, sharing, distribution and reproduction in any medium or format, as long as you give appropriate credit to the original author(s) and the source, provide a link to the Creative Commons licence, and indicate if you modified the licensed material. You do not have permission under this licence to share adapted material derived from this article or parts of it. The images or other third party material in this article are included in the article's Creative Commons licence, unless indicated otherwise in a credit line to the material. If material is not included in the article's Creative Commons licence and your intended use is not permitted by statutory regulation or exceeds the permitted use, you will need to obtain permission directly from the copyright holder. To view a copy of this licence, visit <http://creativecommons.org/licenses/by-nc-nd/4.0/>.

© The Author(s) 2025